Seismic strengthening of reinforced concrete walls in existing buildings with fibre-reinforced polymer materials

Principal investigator: Dr Enrique del Rey Castillo, Senior Lecturer at the University of Auckland.

Other team members: Zhibin Li (PhD candidate), Dr Rick Henry (Associate Professor at the University of Auckland), and Andrew Thompson (Structural Engineer at Holmes Consulting)

Executive summary

Reinforced concrete (RC) buildings constructed prior to the introduction of ductile design requirements may exhibit undesirable seismic behaviour. For RC walls, one such vulnerability is the lack of confinement to end regions that may lead to non-ductile compression failures. To overcome this vulnerability, strengthening of non-ductile RC walls is often required and the addition of confinement to end region concrete can be implemented using carbon fibre reinforced polymer (FRP) laminate and spike anchors. The main issue encountered when applying this strengthening method is the lack of existing design guidance on this confinement method, due to a lack experimental data to validate the approach. The objectives of this study were to:

1. provide the necessary experimental data to quantify the behaviour of concrete confined with FRP laminate and spike anchors,
2. develop a design method to calculate the behaviour of the confined concrete, and
3. verify that this method is applicable to wall boundary region confinement.

Static monotonic axial compression tests were conducted on 75 concrete prisms confined with FRP laminate and spike anchors using various FRP configurations. The most important parameter for both peak strength and deformation capacity is anchor spacing. A simple, analytical method has been developed that appropriately predicts the experimental results. This model was then applied in the design of the FRP strengthening of four concrete walls, and the various FRP configurations were investigated and compared with the behaviour

of the un-strengthened wall. The deformation capacity significantly improved, with the failure of the wall being delayed from about 1% lateral drift to over 2.5%.

Introduction

Reinforced concrete (RC) walls are commonly used as lateral-load-resisting elements of multi-storey RC buildings (Paulay and Priestley 1992). Modern RC walls are designed to exhibit ductile response during earthquakes, but many existing RC walls were constructed prior to the introduction of ductile design requirements in the 1980s. Poor ductility of RC walls was found during the 2010/2011 Canterbury earthquakes (Sritharan et al. 2014), with observed damage attributed to a range of deficiencies in different types of walls (Shegay et al. 2020). Poor drift capacity resulting from concrete crushing at compression toe was identified as one of the common seismic deficiencies of walls built in the 20th century (Kam and Pampanin 2011; Shegay et al. 2020). A typical case of pre-1970s concrete walls is singly reinforced walls using a single layer of reinforcement without transverse confinement was previously assessed (Zhang et al. 2018a; Zhang 2019a). Test results showed the walls experienced concrete crushing that limited drift capacity and walls subjected to a moderate or high axial load ratio experienced axial failure that could lead to building collapse. The poor behaviour of singly reinforced walls tested by Zhang et al was attributed to low deformation capacity of concrete in wall compression toe resulting from lack of confinement.

Seismic strengthening of RC walls with carbon fibre reinforced polymer (FRP) has been extensively investigated to solve various problems, such as poor flexural ductility (Khalil and Ghobarah 2005; Dan 2012; El-Sokkary et al. 2013; Matsui et al. 2014; Matsui et al. 2017) and potential shear failures (Kobayashi 2005; Altin et al. 2013; El-Sokkary et al. 2013; Qazi 2013; Qazi et al. 2015). The FRP strengthening method studied by Matsui et al. (2014; 2017) was shown to be successful to improve drift capacity of singly reinforced walls. Matsui et al investigated wrapping FRP jackets around the wall end regions and anchoring the FRP with steel plates and bolts through the wall thickness to provide confinement to ends of the walls and improve the deformation capacity. Test results illustrated that the drift capacity of the strengthened walls was significantly improved compared to the unstrengthened reference walls.

Instead of using steel plates and bolts to anchor the FRP U-shape laminates, an alternative approach has been proposed using spike anchors, as shown in Figure 1. This type of confinement has been adopted in seismic strengthening of columns shown in Figure 1a) and walls shown in Figure 1b). However, design guidance is limited on confinement using FRP spike anchors. An improved understanding is required on the compressive behaviour of concrete confined with FRP U-shape laminates and spike anchors to improve confidence in strengthening of existing structures such as walls. FRP spike anchors are commonly used in

other applications, such as preventing debonding between concrete and laminates (Kalfat and Al-Mahaidi 2016) and transferring forces from laminate into concrete structures during earthquakes (del Rey Castillo et al. 2018). The use of FRP spike anchors for confinement in elements such as walls has not been extensively investigated. Currently, confinement with FRP consist of a jacket wrapping around the entire section (e.g. columns) and the axial behaviour of concrete in this confinement has been previously studied in detail (Fardis and Khalili 1982; Lam and Teng 2003; Moran et al. 2019). The design-oriented axial stress-strain model of concrete confined by FRP jackets developed by Lam and Teng (2003) was accepted in ACI 440 (2017) and is widely used. In order to understand the compressive response of FRP-confined concrete with laminate and spike anchors, a series of static monotonic axial compression tests were conducted on concrete prisms. The prisms simulated the end region of strengthened RC walls and provide data that could be used to validate stress-strain models and design recommendations that could be implemented when strengthening poorly confirmed RC walls.
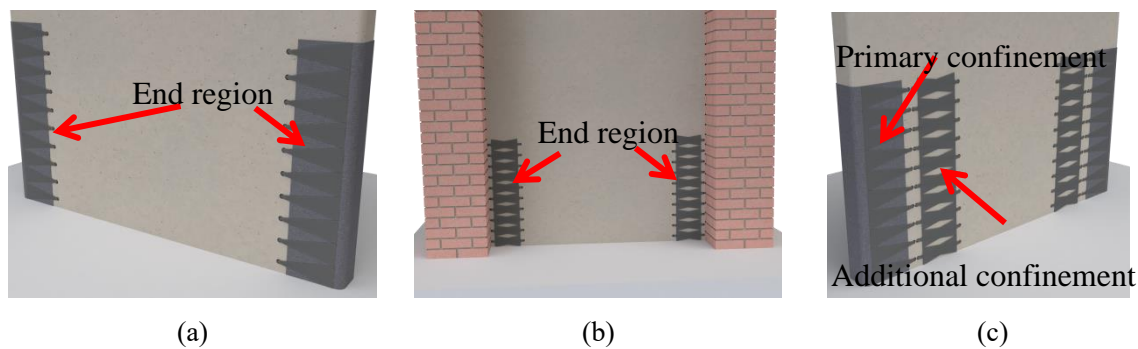

| (a) | (b) | (c) |

Figure 1 Wall strengthening with FRP -confinement: (a) Laminate and spike anchors; (b) Only spike anchors; (c) Multiple confinements

Experimental programme part A - Prisms

Prism design and test matrix

A total 75 concrete prisms were tested by applying uniform axial compression. The test prism design is shown in Figure 2 for confinement configuration A (U-shaped FRP laminates and one-sided FRP anchors) and in Figure 3 for configuration B (FRP anchors on two sides). The prism width (*b*) was equal to 150 mm for all prisms, which represented the thickness of walls that are generally constructed before ductility requirement was introduced (Zhang et al. 2018a; Zhang 2019a). The prism length (*l*) was varied during the test to create different cross-sectional aspect ratios. To reduce the effect of eccentricity in compression while allowing more options of distributing the spike anchors, the prism height (*H*) was designed as 360 mm.
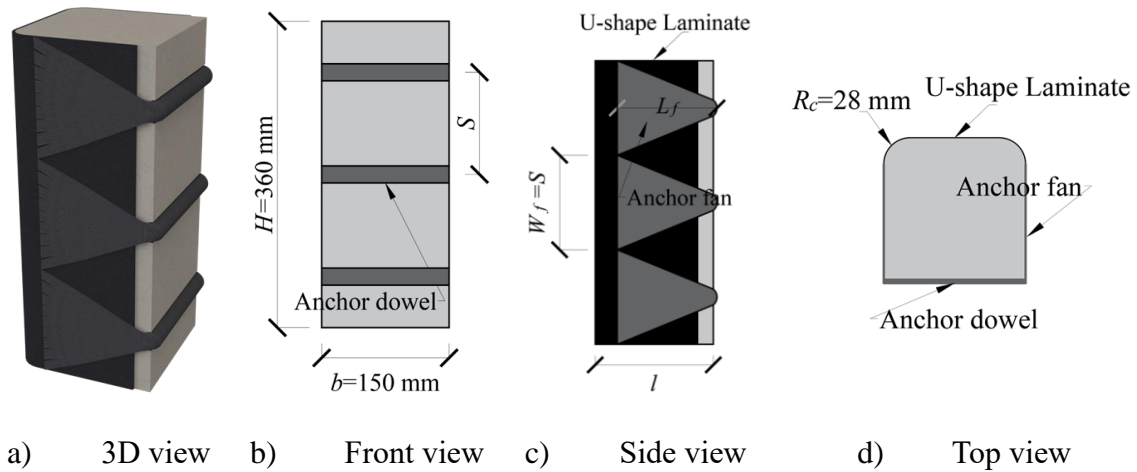
| a) | 3D view | b) | Front view | c) | Side view | d) | Top view |

Figure 2 Drawings of concrete test prisms confined by FRP U-shaped laminates and one-sided FRP anchors (confinement type A)

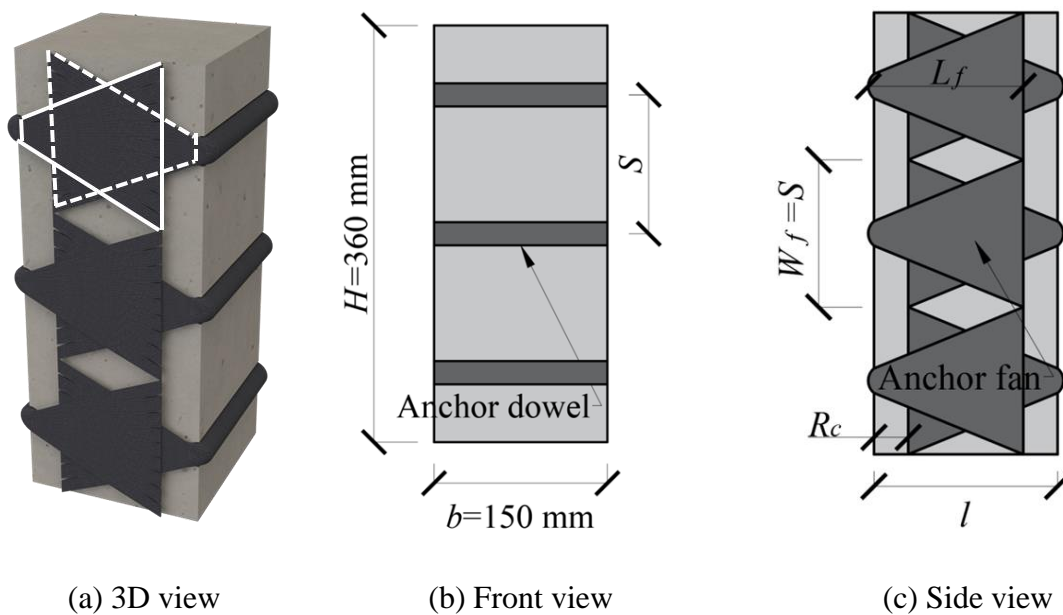| (a) 3D view | (b) Front view | (c) Side view |

Figure 3 Drawings of concrete test prisms confined by FRP anchors on two sides (confinement type B)

The variable tested for the confinement configuration A and B are summarized in Table 1 and Table 2 respectively. Each group ID represents a type of confinement configuration. The letter in the group ID denotes the cross-sectional aspect ratio of prisms, either S for square or R for rectangular cross-sections. The square cross section had a prism length (l) of 150 mm, resulting in a cross-sectional aspect ratio of 1. The rectangular cross-section had a prism length (l) of 200 mm, resulting in a cross-sectional aspect ratio of 1.33. The reference unconfined

concrete prisms were labeled a S and R for square and rectangular cross sections. The anchor spacing (S) was varied between 90 mm, 120 mm and 180 mm, the cross-sectional area (A_d) was varied between 14 mm^2, 28 mm^2 and 56 mm^2, the fan length (L_f) is defined as the length of lateral projection of the fan, while the fan width (W_f) is the vertical projection.

Material properties

The concrete properties are reported in Table 3 and Table 4 for configurations A and B respectively. The FRP and epoxy materials were the same for both configurations, reported in Table 5 and Table 6 respectively.

Test set-up and instrumentation

A 2000 kN testing machine and three IDS UI-3280CP Rev. 2 industrial cameras were used as shown in Figure 4, recording load, displacements and strains.
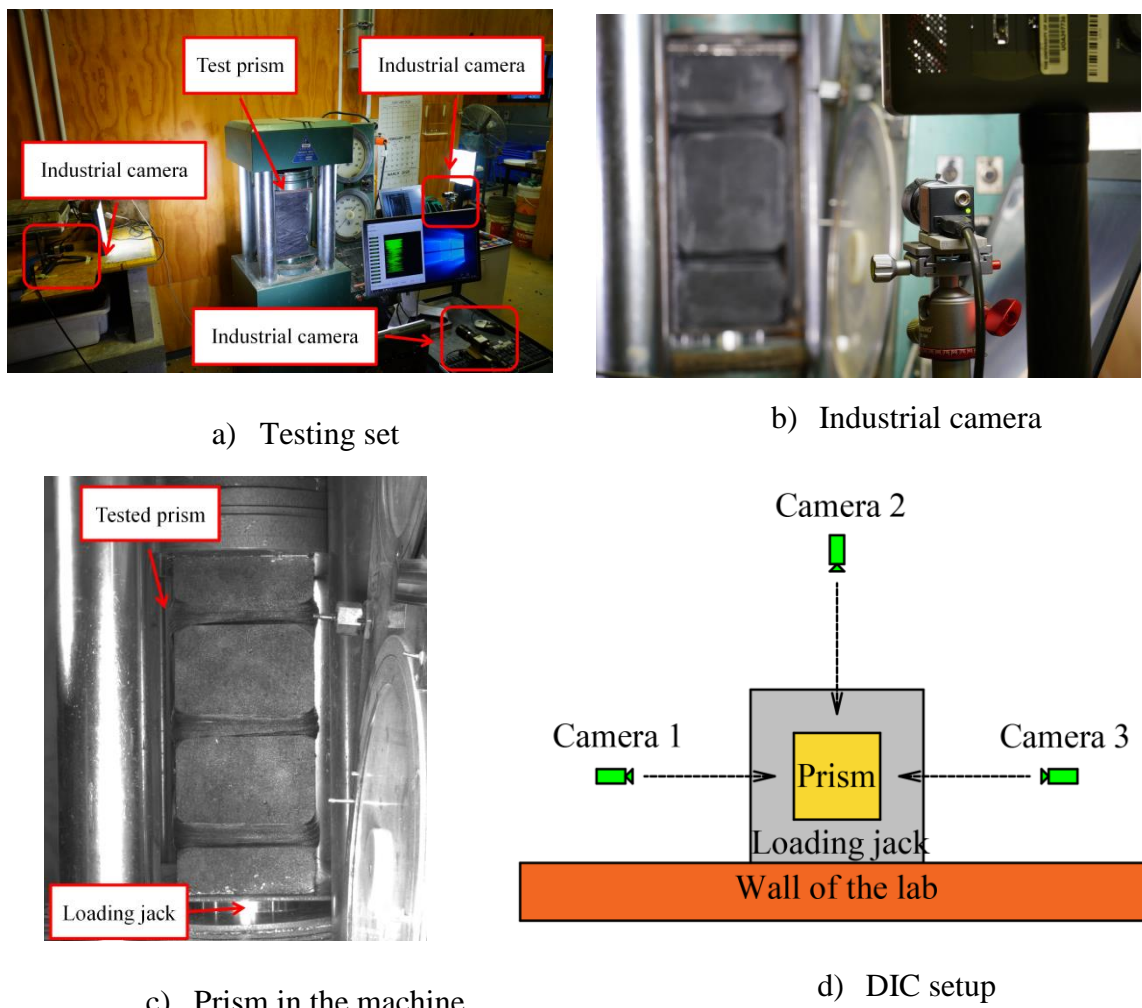

a) Testing set

b) Industrial camera

c) Prism in the machine

d) DIC setup

Figure 4 Test set-up and instrumentation

Prisms behaviour and test results

The behaviour of the prisms, the stress-strain response, and the calculation and design method are highly dependent on the failure mode, with some examples being shown in Figure 5. Concrete failure and fan debonding (a) and b)) result in more brittle response, and should be avoided. The anchors should be placed close enough to result in fibre rupture, shown in c). The summary of the failure mode for each prism is in Table 7 and Table 8.

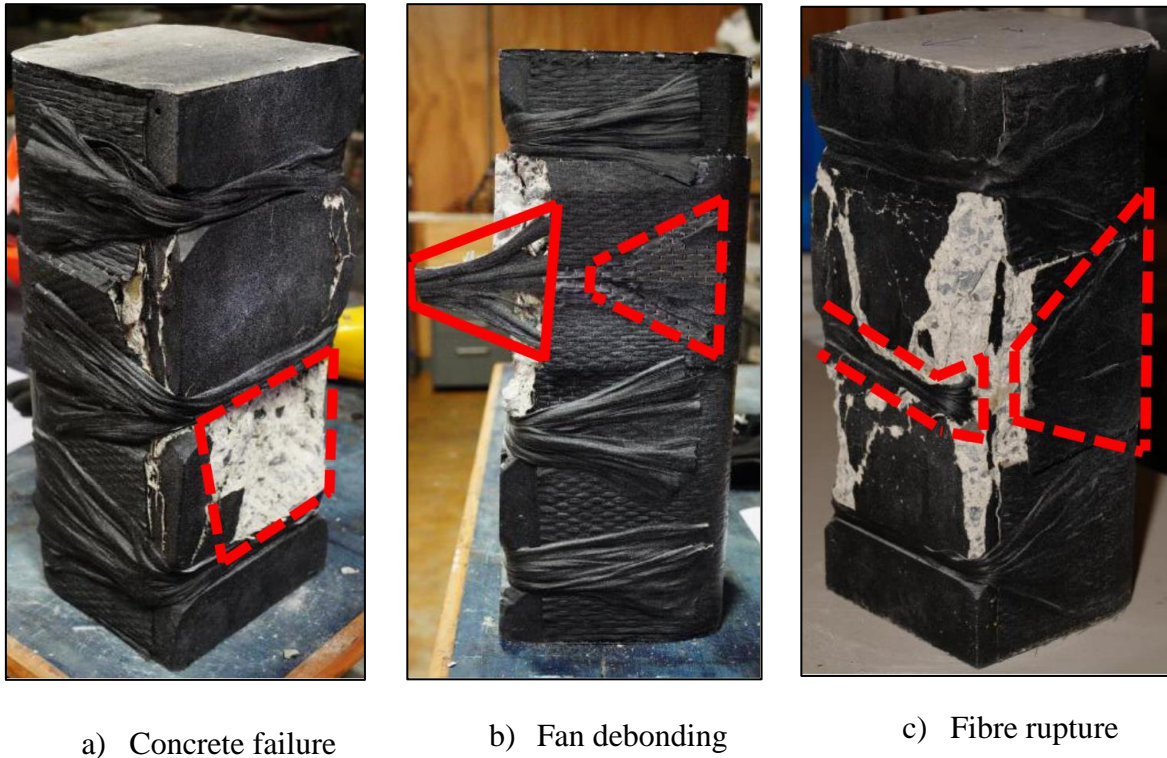a) Concrete failure   b) Fan debonding   c) Fibre rupture

Figure 5 Failure modes observed on the prisms

The photos taken by IDS UI-3280CP Rev. 2 industrial cameras were translated into strain of concrete and FRP with TRIDENT V3.0, a DIC processing Matlab (2015) GUI developed by the Center for Advanced Composite Materials (CACM) at the University of Auckland (Stubbing 2013; Stubbing 2016). The axial strain of each prism was obtained from the middle portion of the prism and synchronized with the load by using the recorded photos. The axial stress-strain curves of confined prisms are shown in Figure 6 and Figure 7. Adequate deformation capacity was achieved mostly when anchors were placed 90 mm apart, with moderate deformation being obtained at 120 mm apart and insufficient capacity being achieved when the anchors were installed 180 mm apart.
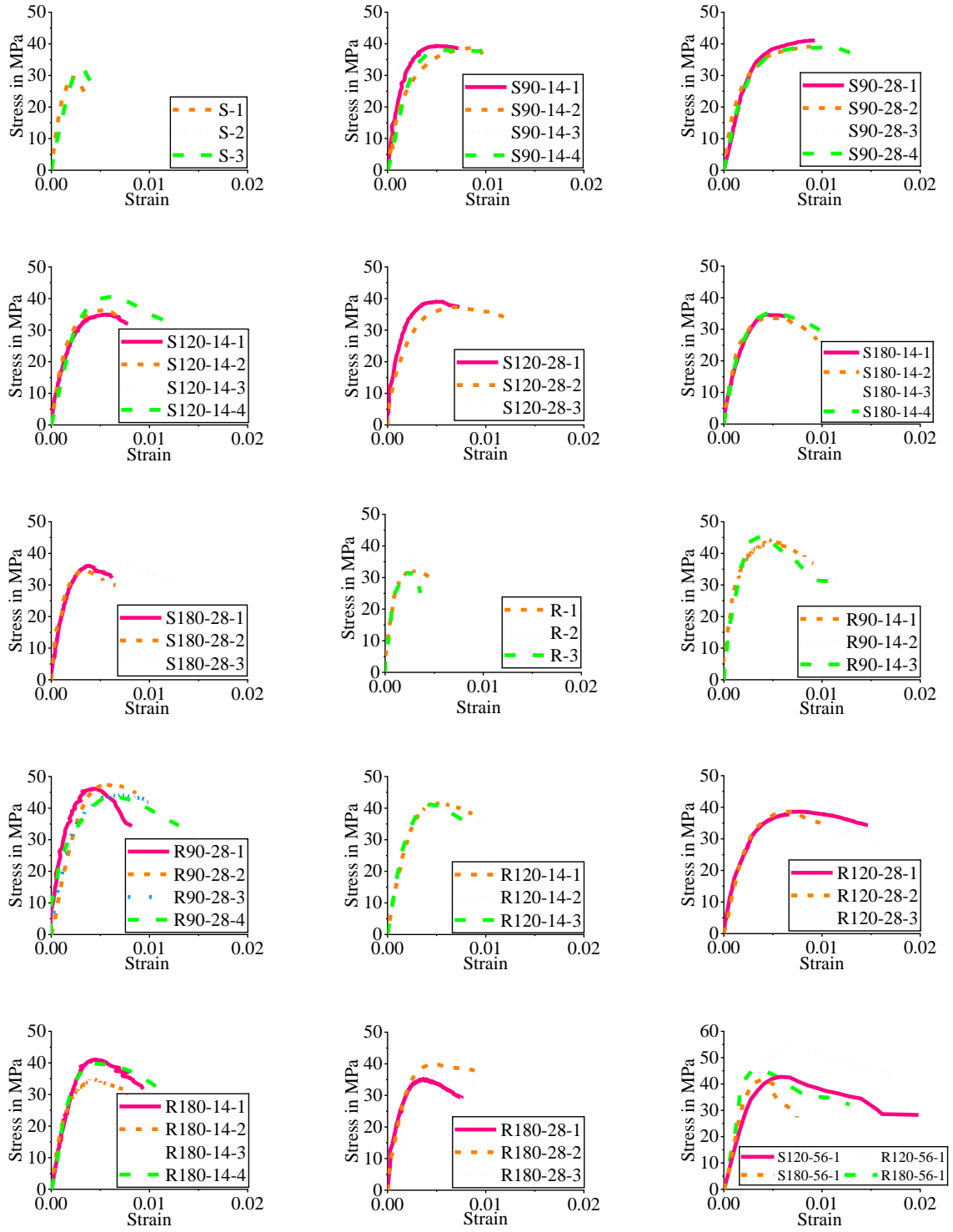
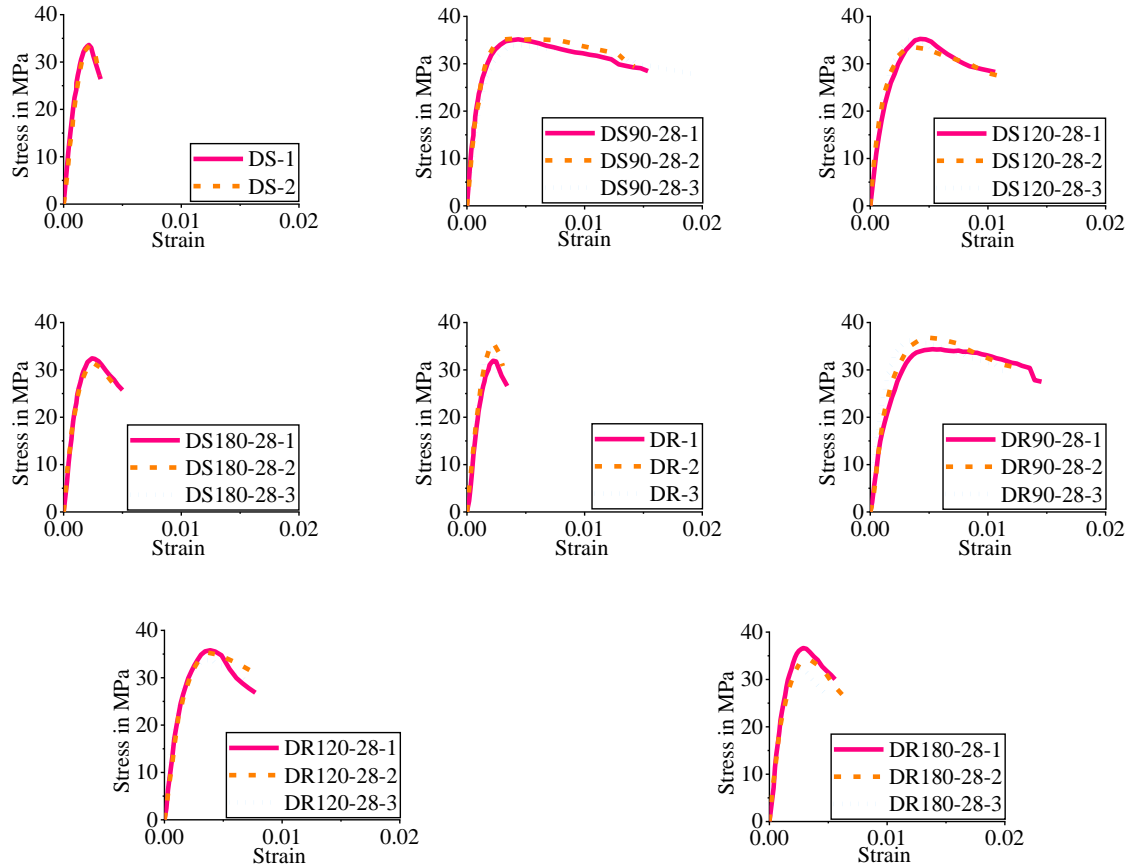Figure 6 Axial stress-strain curves for configuration A

Figure 7 Tested axial stress-strain curves for configuration B

The mechanical properties of the concrete prisms are summarized in Table 10 and Table 9for configurations A and B respectively. The properties include peak strength, strain at peak, stress at failure and failure strain (f_{co}, ε_{co}, f_{cu} and ε_{cu}). The ratios of average mechanical properties of confined prisms ($f_{cp,ave}$, $\varepsilon_{cp,ave}$ and $\varepsilon_{ccu,ave}$) to that of unconfined prisms ($f_{co,ave}$, $\varepsilon_{co,ave}$ and $\varepsilon_{cu,ave}$) with the same cross-sectional aspect ratio are also reported to demonstrate the improvement in the mechanical properties of confined concrete.

Stress-strain model

The stress-strain model was developed based on the confinement pressures on the FRP as the concrete expands when subjected to compression forces. A schematic representation of these forces for both confinement types is included in Figure 8 and Figure 9. Including the full formulation of the model would be inappropriate due to time constrains, but it's included in the attachments and it's being submitted for publication soon. A visual comparison between the experimental data and the analytical prediction is also included in Figure 10. The coefficient of determination (R^2) is annotated for each curve, with an average as 0.96, a standard of deviation of 0.001 and coefficient of variation as 0.1%. The experimental and the analytical
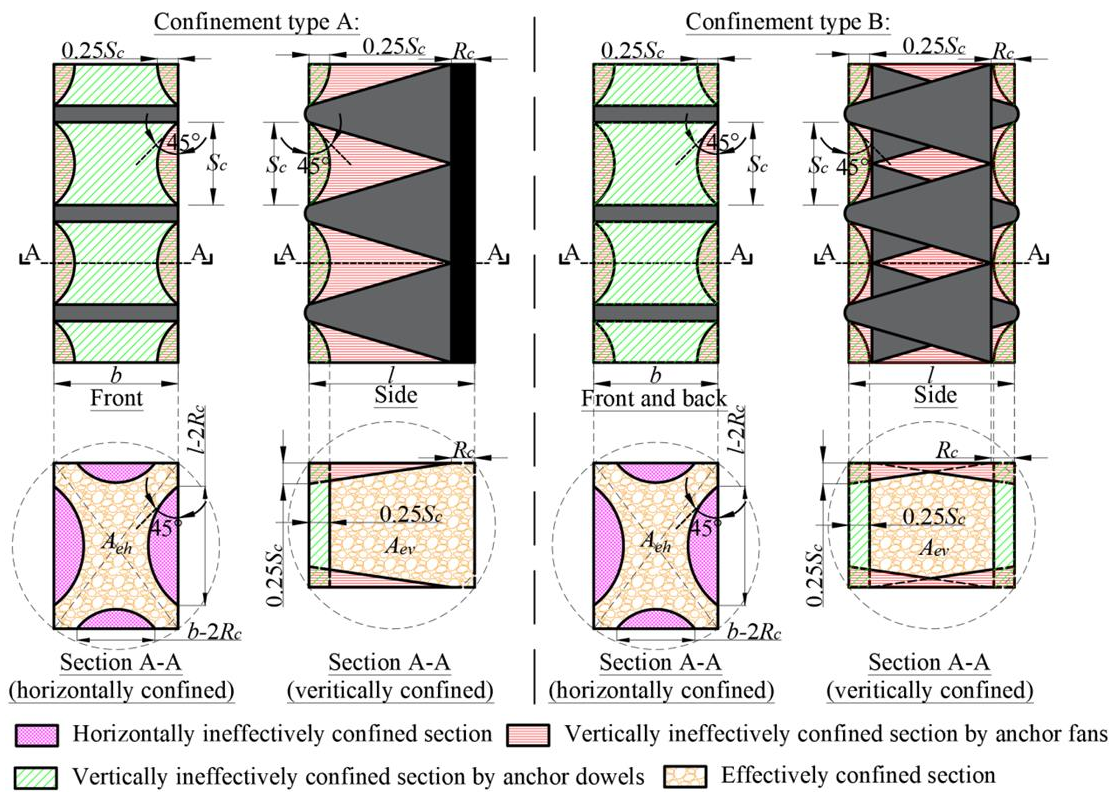
curves generally agree with each other, with the inaccuracy being mainly a result of the linear regressions discussed above.
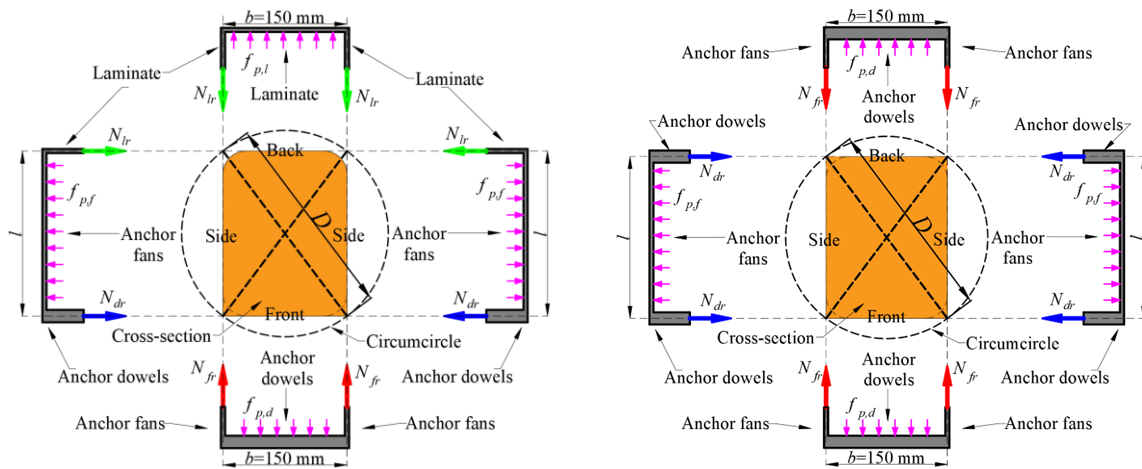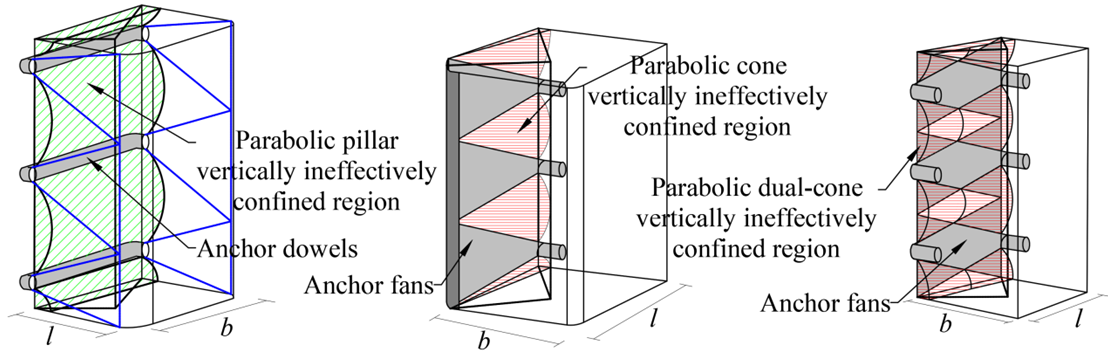

Confinement type A   Confinement type B

Figure 8 Different confinement elements in cross-sectional view
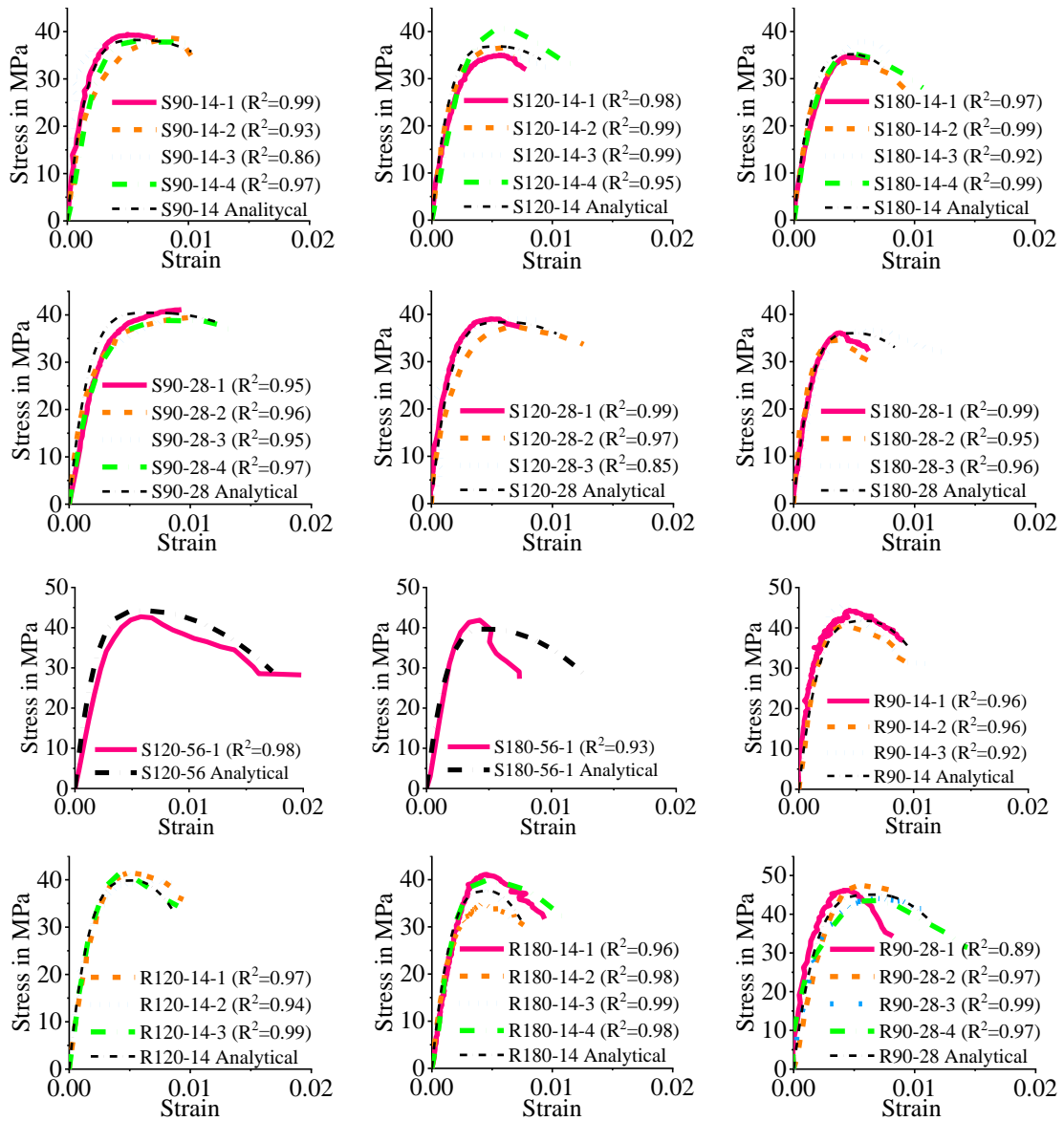

(a) Effectively and ineffectively confined sections

(b) Vertically ineffectively confined region in 3D view

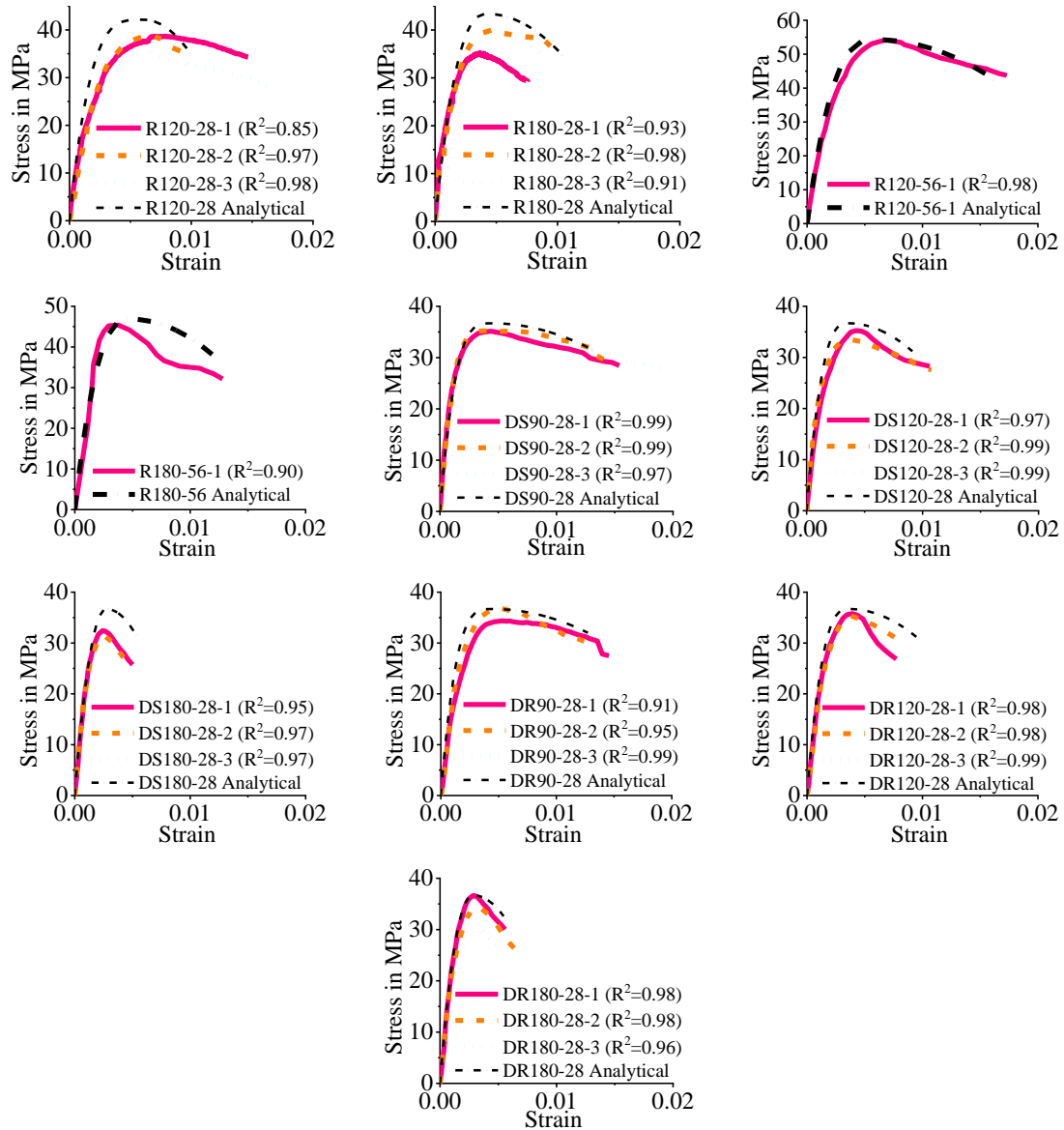Figure 9 Classification of the confined sections

Figure 10 Comparison between tested and predicting stress-strain curves

Experimental programme part B – Walls

Wall design and test matrix

Two types of confinement have been investigated, corresponding to confinement A and B from the prisms. These two configurations are schematically represented in Figure 5. Six identical full-scale pre-1970s singly RC walls were tested, with the test matrix summarized in Table 11. Two of these walls were tested previously by Zhang et al(Zhang et al. 2018b; Zhang 2019b), and are considered the reference walls subjected to different axial load ratios, namely 10% and 3.5%. The dimension of the wall panel was 150 (wall thickness) ×1920 (wall length) × 3840 (wall height) mm×mm×mm. The detailing of the walls and the FRP strengthening design are detailed in Figure 12. The main objective of this test programme was to evaluate the

global behaviour of the FRP-strengthened wall and the influence of the FRP, but also to investigate the difference between the various confinement strategies to optimise the design.
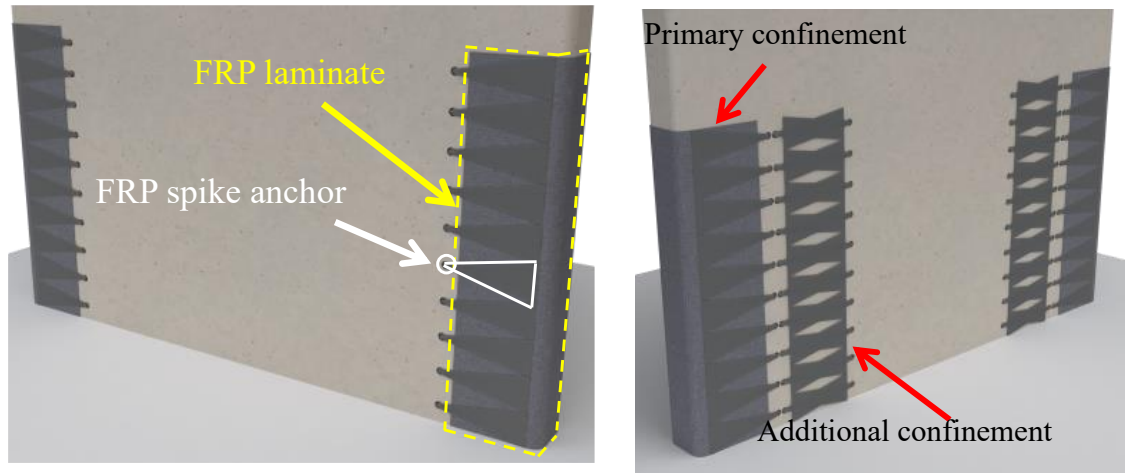
a) Laminate and spike anchors (confinement type A)

b) Only spike anchors (confinement type B)

Figure 11 FRP confinement con walls
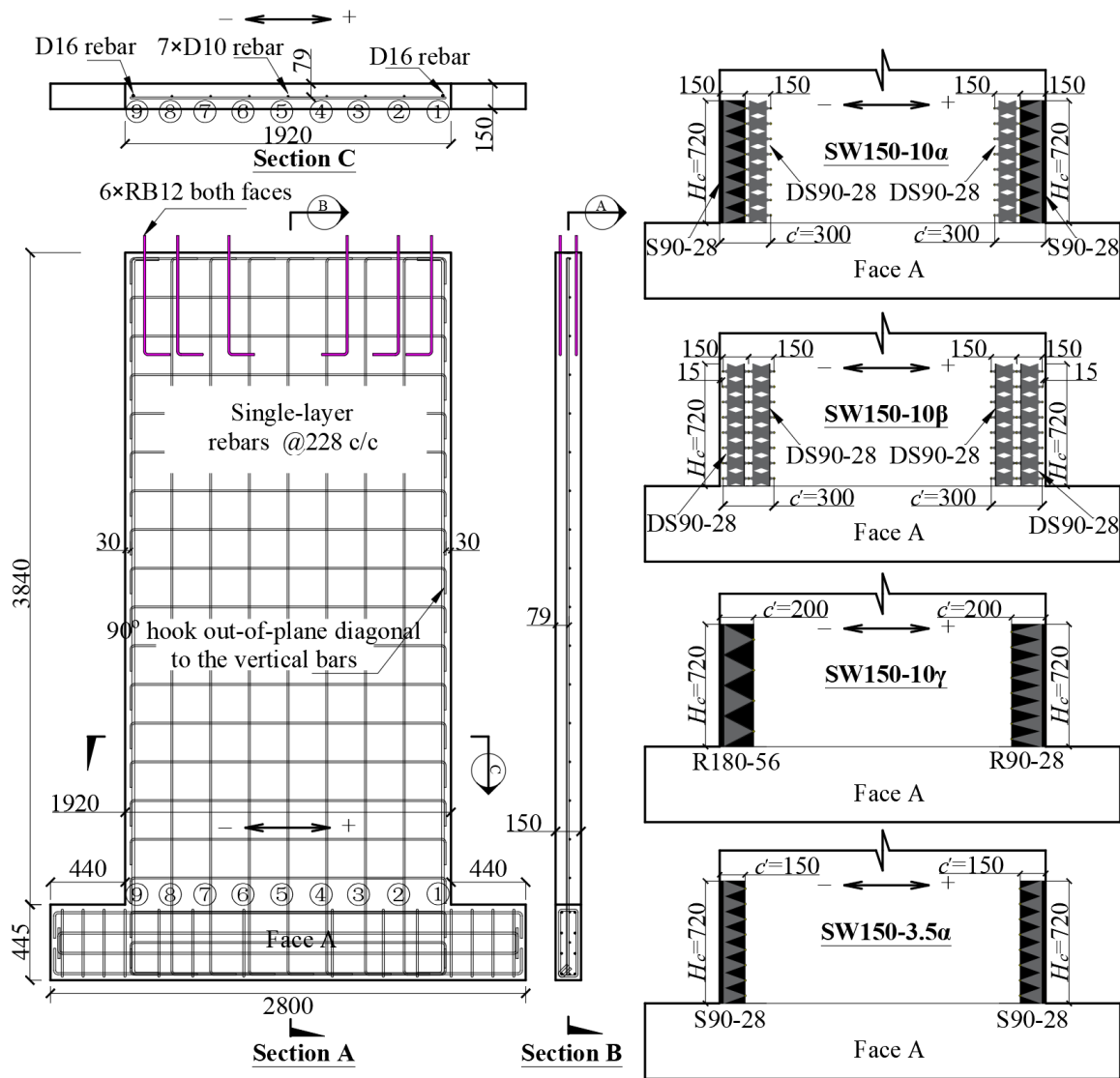
Figure 12 Wall detailing and strengthening design (unit: mm)

Wall fabrication, FRP installation and material properties.

Details of the wall construction and FRP installation are included in Figure 13. The FRP and resin materials are the same as for the prisms. The concrete and steel properties are reported in Table 12.

(a) Reinforcement into formwork

(b) Pouring concrete

(c) Drilling holes to install FRP spike anchors

(d) Grinding for rounded corners before wrapping FRP

(e) Saturating the FRP laminate with epoxy resin

(f) Wrapping the U-shape FRP laminate

(g) Installing FRP spike anchors

(h) Placing sandwich cover upon the FRP spike anchors.

Figure 13 Wall fabrication and FRP installation

Testing setup, loading protocol and instrumentation

This setup included five main parts namely the safety frame, the foundation block pair, the loading beam, the axial load system and the actuator, as illustrated in Figure 14a. The safe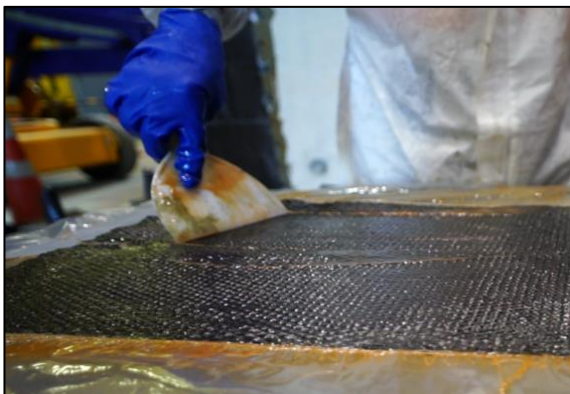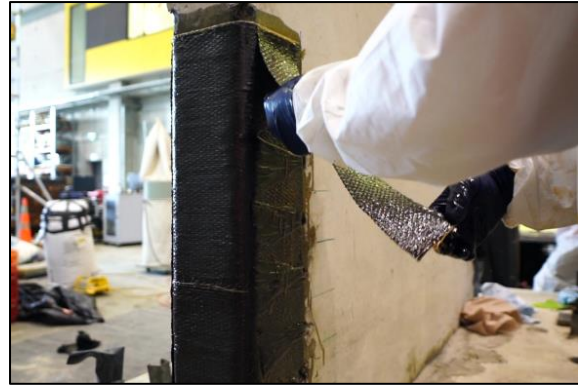ty frame consisted of a universal steel column and a C-channel cross-sectional steel safety beam couple connecting the strong wall, the strong floor and each other, in case of the possible out-of-plane fall of the wall panel at failure. The foundation block pair was made using heavily reinforced 60 MPa concrete (Zhang et al. 2018b; Zhang 2019b) and post-tensioned to the strong floor with a gap in between for the wall to slot in, which was then filled with 60 MPa grout and post-tensioned together. The loading beam was a universal steel beam with stiffeners, mounted and bolted on top of the wall as shown in Figure 14b. The loading beam connected the wall, the axial load system and the actuator. The axial load system consisted of the axial load rig, four post-tensioned bars, four hydraulic jacks and four load cells, standing on a swivel or hinge to allow for in-plane rotation.
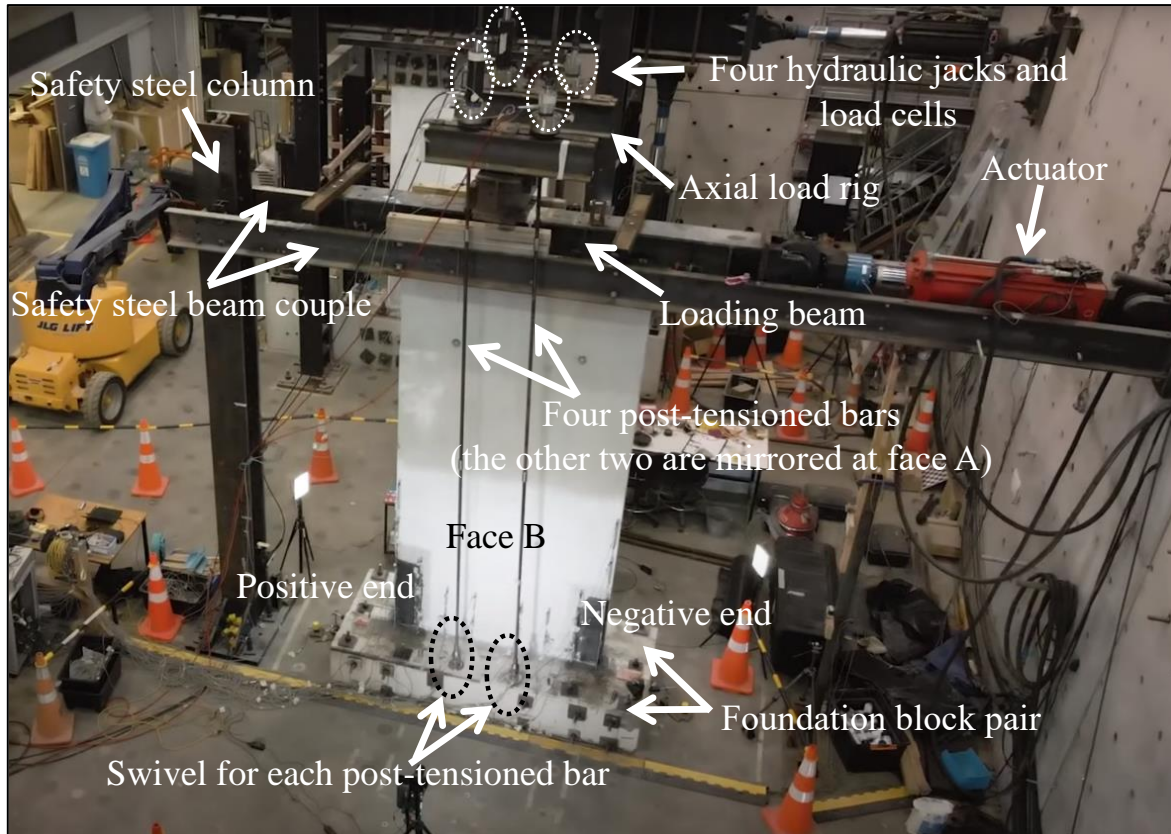
a) Overall photograph
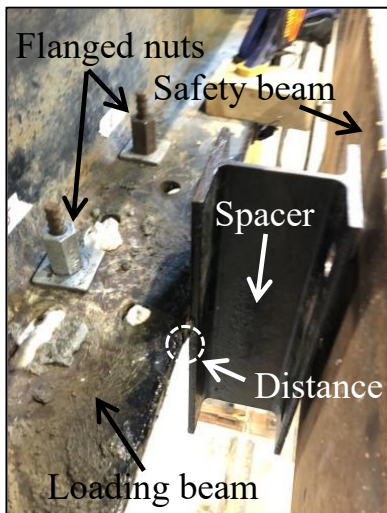
b) Spacer
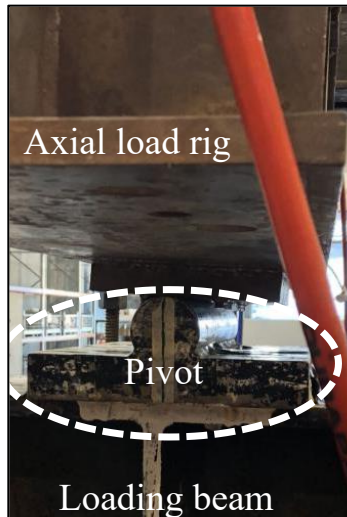
c) Pivot

d) swivel

Figure 14 Test setup

The walls were subjected first to a constant axial load, equal to 864 kN for SW150-10, SW150-10α, SW150-10β and SW150-10γ, as the axial load ratio was 10%, and 302 kN for SW150-3.5 and SW150-3.5α for an axial load ratio of 3.5%. Then the reversed cyclic load was applied application, pausing at positive wall drift amplitude, zero wall drift, negative wall drift

amplitude and zero wall drift to record damage and other observations and take pictures for DIC. The lateral loading application was carried on in three stages. Force-controlled mode was adopted in stage one of the reference walls, including three cycles with different wall drift levels depending on the force equaling to 1/4, 1/2 and 3/4 the nominal strength of the walls(Zhang et al. 2018b; Zhang 2019b). The objective of stage one of the strengthened walls was to capture the stiffness before and after cracking so small displacements were used in this phase. Test results of the reference walls showed that the wall drift at cracking was recorded down to 0.05%(Zhang et al. 2018b; Zhang 2019b), so the stage one loading protocol was determined as displacement-controlled model with 0.005%, 0.01% and 0.075 % wall drift levels in order, with two cycles each level. Stage two protocol was determined as displacement-controlled mode to start at a drift where the yielding was presumed and consistent with the one of the reference wall testing, being 0.15%, 0.20%, 0.25%, 0.35%, 0.50%, 0.75%, 1.0%, 1.5%, 2.0% and 3.0% wall drift levels in order(Zhang et al. 2018b; Zhang 2019b), following ACI ITG-5.1-07(ACI 2007).

Four load cells were placed in the axial load system to measure the axial load readings. A load cell and a linear variable differential transformer (LVDT) were in-built in the actuator to record the lateral load and displacement respectively. Two draw wires (DWs) were used to monitor the displacement of the wall and three Linear Variable Differential Transformers (LVDTs) were used to record potential sliding or uplifting of the wall with respect to the strong floor. Digital image correlation (DIC) cameras and a matrix of linear pot (LP) gauges were deployed on each wall face at the regions close to the wall base to record the wall movement and deformation, as shown in Figure 15. Five cameras were deployed at 1200 mm from the wall surface targeting different sections and numbered from camera 1 to camera 5. Camera 1 and 5 targeted the framed sections on the two sides at positive and negative ends, respectively. Cameras 2 and 4 targeted the boundary regions on face A at positive and negative ends, respectively. Camera 3 targeted the entire face A up to a level of about 1700 mm. Black-in-white or white-in-black speckle patterns were paint on the target sections to help recognize and track the displacement or deformation of the target sections. These cameras shot in pace with the loading protocol, shooting before and after the axial application and shooting at the pauses at positive amplitude, zero displacement, negative amplitude and zero displacement of the first cycle of each wall drift level.
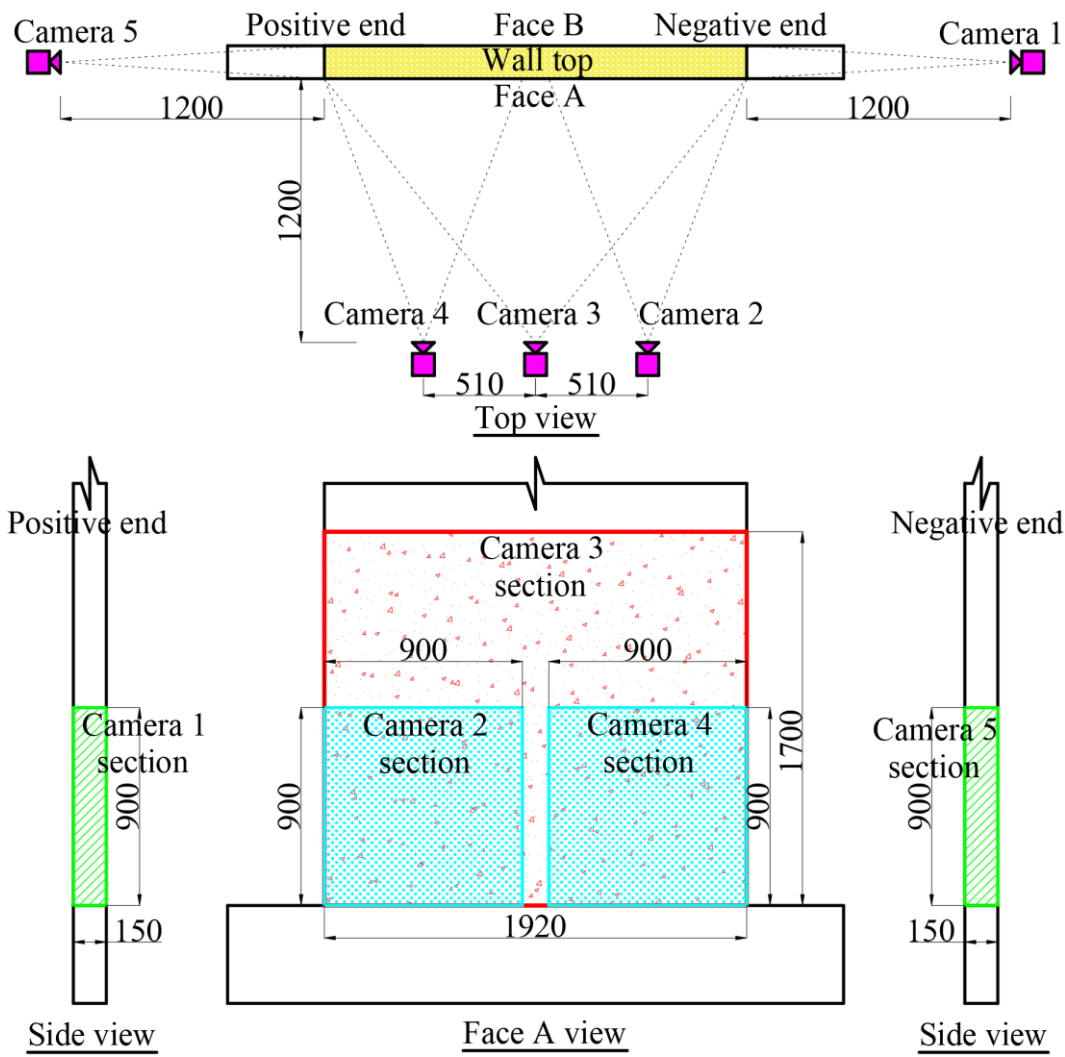
(a) Camera positions and target sections
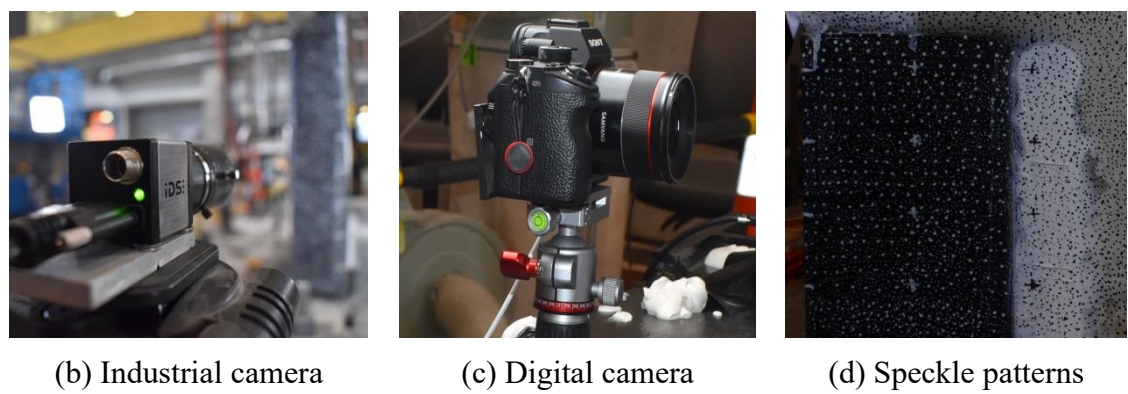
(b) Industrial camera   (c) Digital camera   (d) Speckle patterns

Figure 15 DIC hardware deployment

A linear pot gauge as the one shown in Figure 16(a) is made with a two-end piston and an in-built sensor to measure the distance between the two ends. The linear pot gauges were deployed on face B of the plastic region of the walls, bolted to metal threaded rods embedded into the wall. The linear pot measures the displacement of the two ends, which is the deformation of the wall within the embedded positions. The metal rods cannot be installed through the FRP, which also affected the linear pot positions, as shown in Figure 16 (b). Every

linear pot gauge was numbered for each tested wall, with different gauge length of 270 mm, 400 mm or 810 mm.
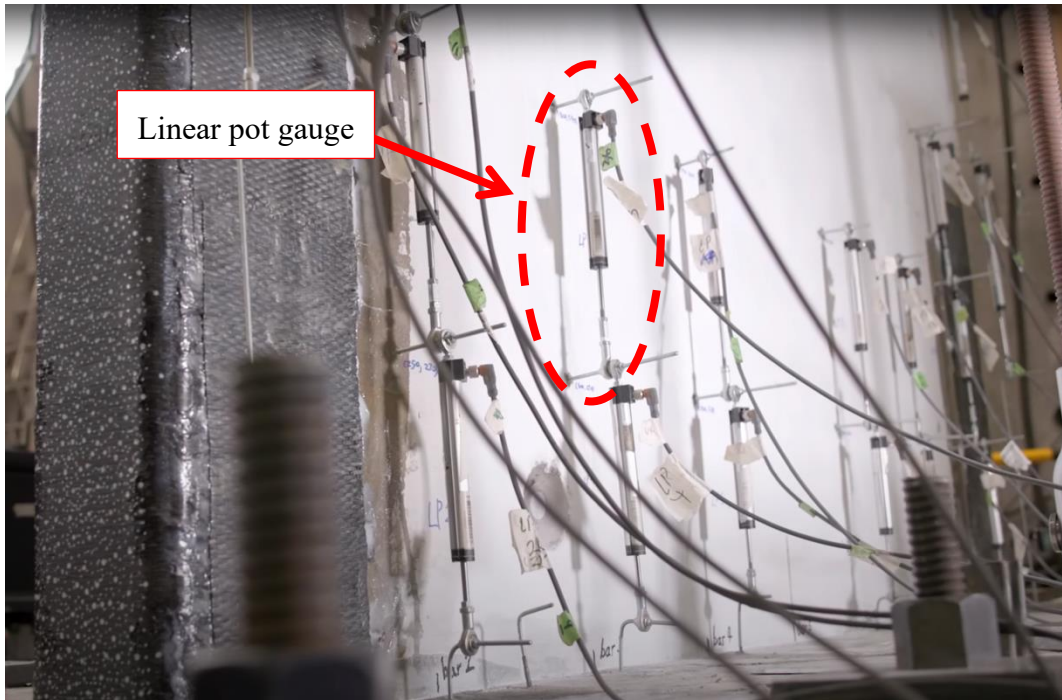
(a) Photos of linear pot gauge gauges on face B
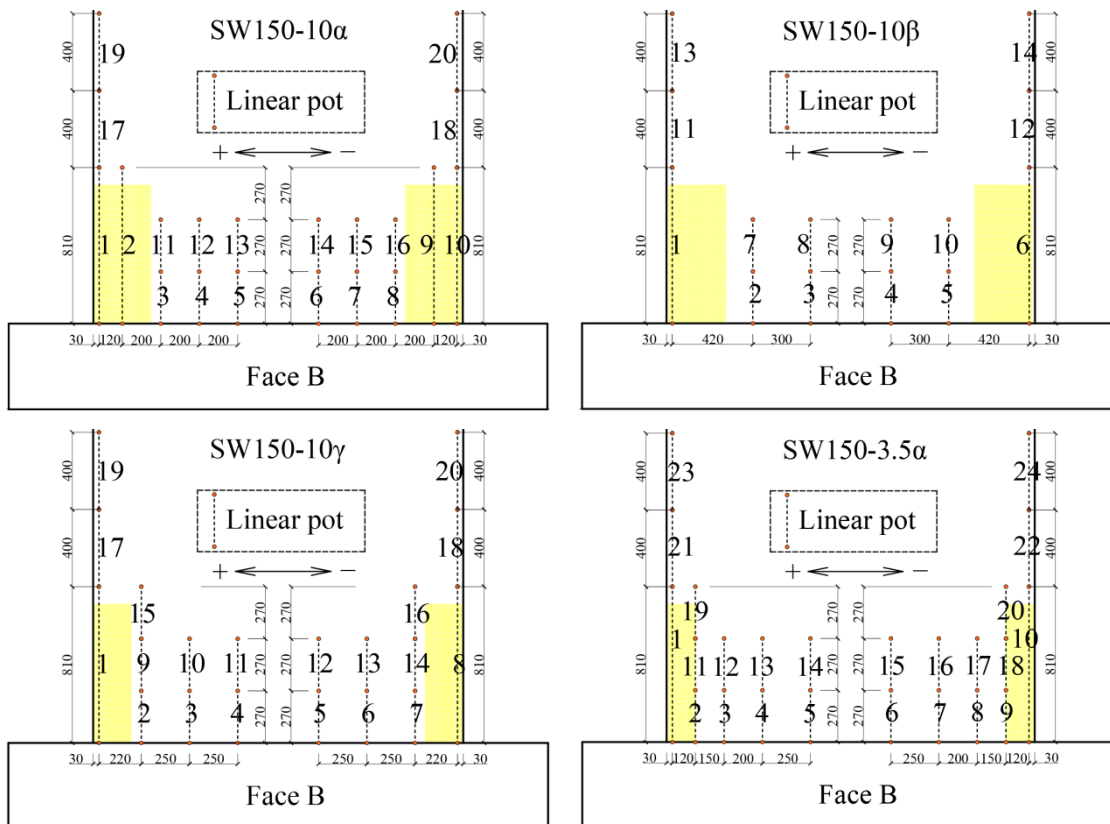
(b) Linear pot gauge position

Figure 16 Linear pot gauge deployment layout

Test results

The load-displacement curves (hysteresis curves) of the reference walls and the strengthened walls are plotted in Figure 17, where some of the key test observations are marked for both positive and negative ends to indicate when these observations were firstly observed. The photos of the key test observations are plotted in Figure 17.

The improvement in drift behaviour observed in the strengthened wall subjected to 3.5% axial load ratio (SW150-3.5α) compared to the reference wall (SW150-3.5) was less significant than in those subjected to 10% axial load ratio. Controlling the axial load was complex, difficult, required a significant exertion by the researchers, and was prone to issues and mistakes. SW150-3.5α was the first FRP-strengthened wall tested by the team and, despite the utmost care taken to avoid issues, some issues happened in the cycle of 0.15% when testing SW150-3.5 and in the cycles of 0.35% and 0.5% when testing SW150-3.5α, leading to larger axial loads than the determined loading protocols. As a consequence, the lateral loads were larger than expected, so the data of these cycles might not reflect the realistic behaviour of the walls and the data from these cycles are not discussed. The main conclusions related to the overall behaviour of the walls were not affected by these cycles, because the focus of this study is preventing axial failure and improving the wall drift capacity with FRP, which was assessed based on the later cycles with bigger wall drift levels. The load started decreasing at 1.0% drift, and further reduced by rebar fracture at 2.0% drift, but axial failure was not observed in this wall. However, the unexpected out-of-plane (OOP) rotation shown in Figure 17(i) was observed at the finishing of the 2nd cycle of 1.5%, resulting in the first load loss in the 3rd cycle of 1.5%. This behaviour was mainly a result of the improperly designed test setup, mainly the excessively large gaps between the loading beam and the safety beam couple, which was fixed in subsequent tests.

The drift behaviour of the walls subjected to 10% axial load ratio was improved significantly following the strengthening. Compared to the reference walls, the strengthened walls SW150-10α, SW150-10β and SW150-10γ retained a residual load of around 60-70% of the peak load (maximum load) even after the cycles with a target wall drift level of 3.0% were complete. This residual load was achieved despite all the rebars being fractured, but axial failure was prevented, as can be seen in Figure 17 (b-d). This behaviour is significantly more ductile and offers more redundancy and protection against earthquake loads than the behaviour observed in the reference wall. After all the rebars had fractured, the SW150-10α wall was subjected to the maximum lateral displacement allowed by the equipment, resulting in a target wall drift level of positive 4.5% and negative 3.5%. This extreme loading scenario did not result in any significant further loss of load or any distinct further damage being observed, as is shown in Figure 17 (b). The various strengthening options (α, β or γ) resulted in different behaviour, mainly in the FRP confinement and in the confined concrete. The load loss SW150-10α was started by rebar fracture, followed by rupture of the FRP U-shape laminate forming the primary confinement, which indicates that the primary confinement had failed. However,

no reduction of the load occurred when the FRP U-shape laminate ruptured because the secondary confinement continued providing deformation capacity to the confined concrete. By contrast, the first observed load loss of wall SW150-10β was caused by concrete crushing, rather by bar fracture. The failure progressed with rebar fracture and then rupture of the lowest FRP anchor dowel. Finally, SW150-10γ, like SW150-10α, experienced first rebar fracture followed by FRP laminate debonding and further rebars fracturing. The FRP confinement failed when the FRP laminate debonded (VII), and the load loss was observed because SW150-10γ had no secondary confinement like SW150-10α to provide further redundancy – providing a secondary confinement is thus recommended. Web concrete spalling between and close to the FRP confinements was observed at the 2nd cycle of 3.0%, although with a limited load loss associated.
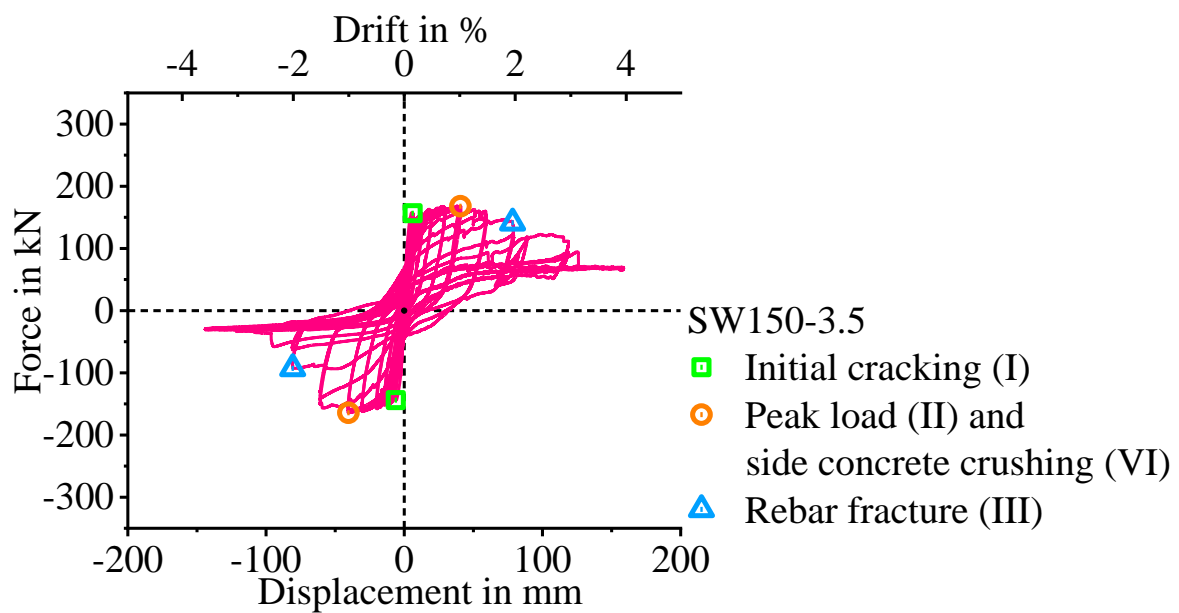
(a) SW150-3.5
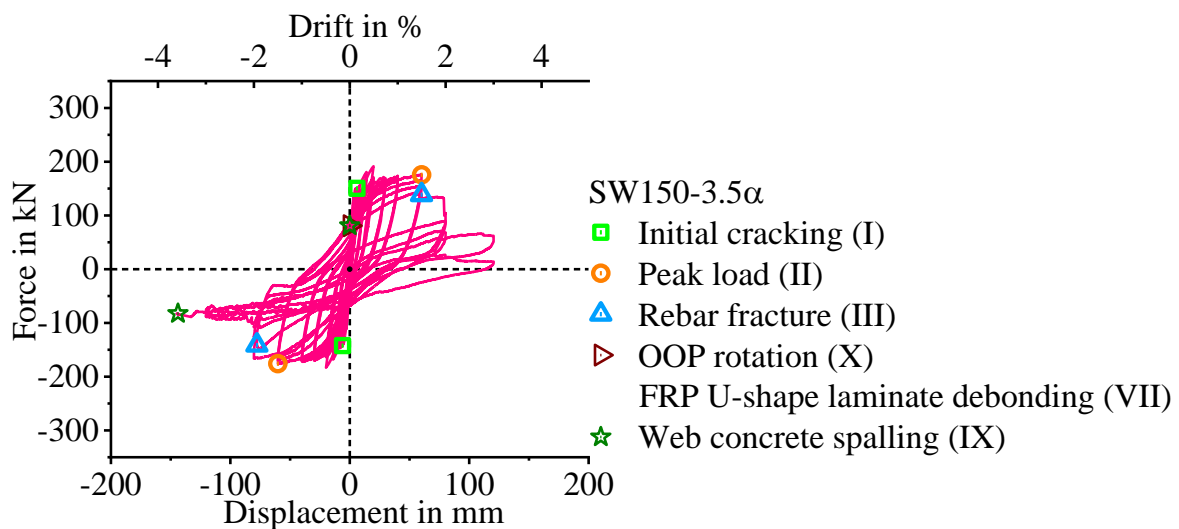
(b) SW150-3.5α.
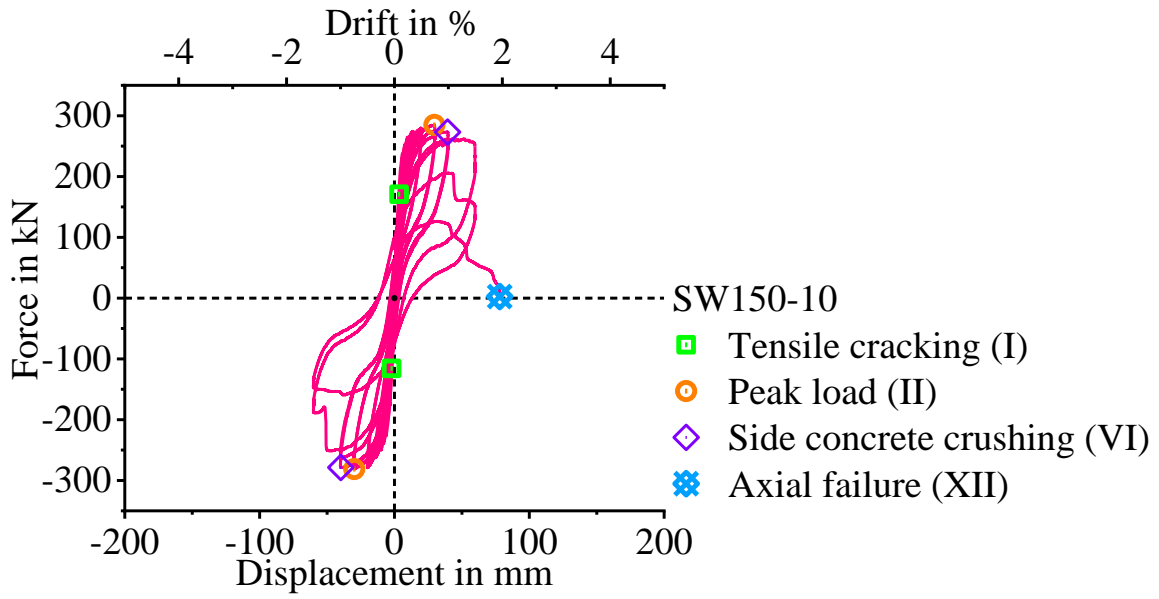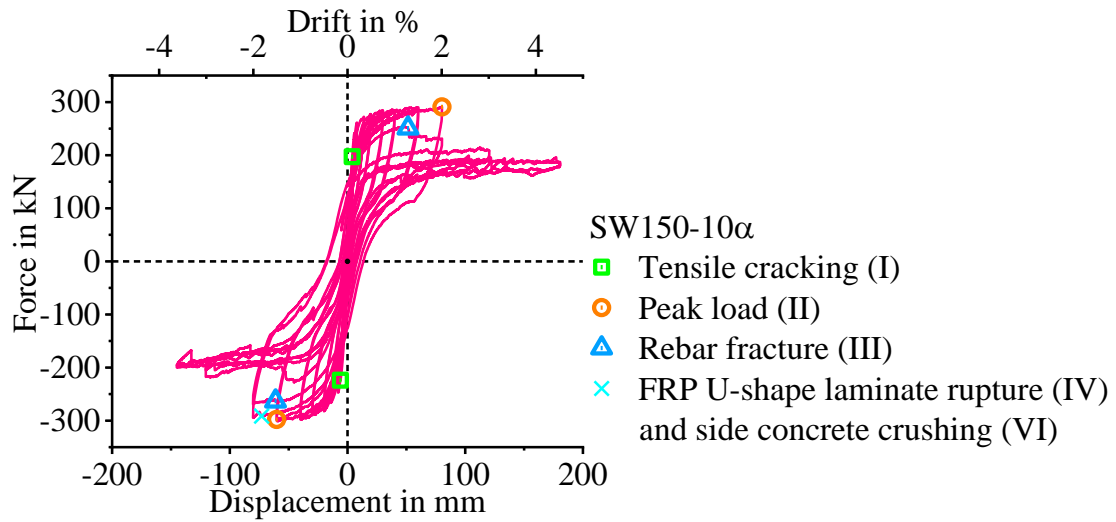
(c) SW150-10

(d) SW150-10α
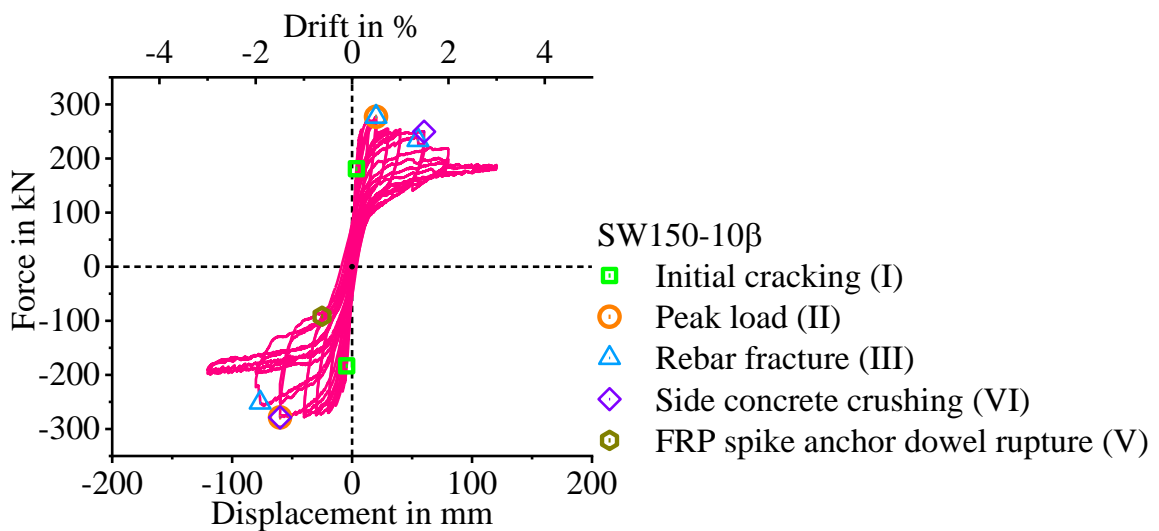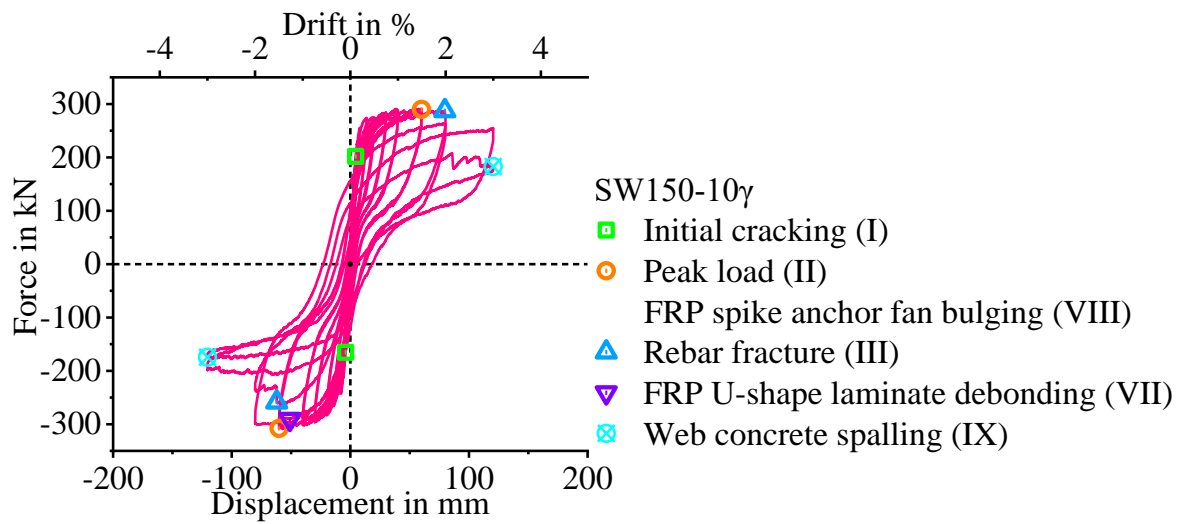
(e) SW150-10β

(f) SW150-10γ

Figure 17 Hysteresis loops
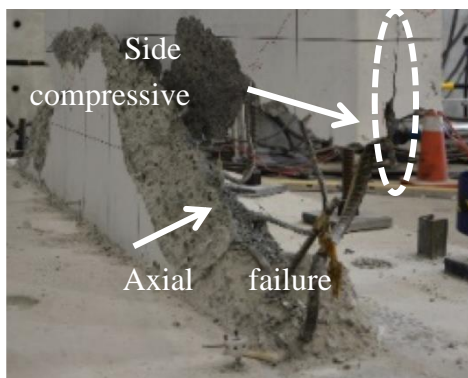
a) Axial failure of SW150-10
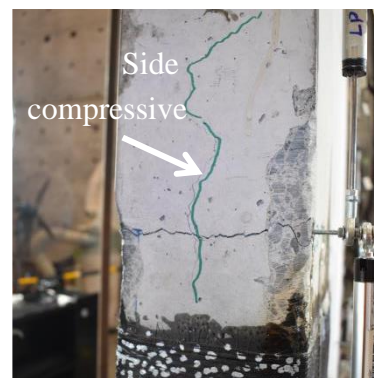
b) Side compressive cracking
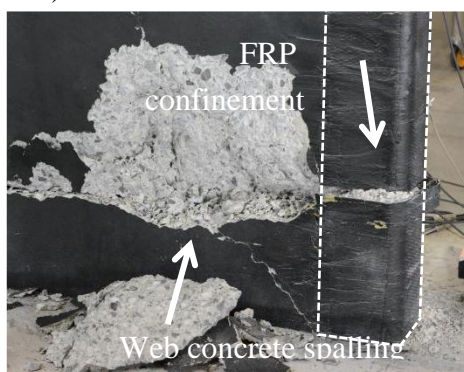
c) Web concrete spalling
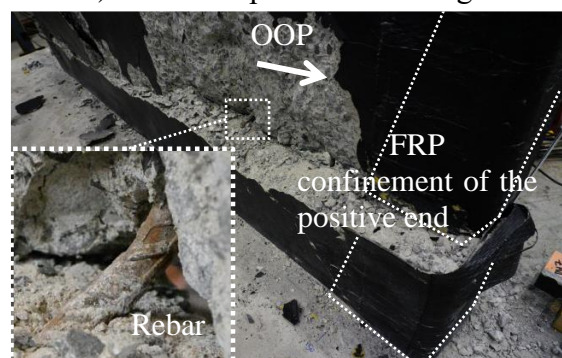
d) OOP rotation with rebar buckling
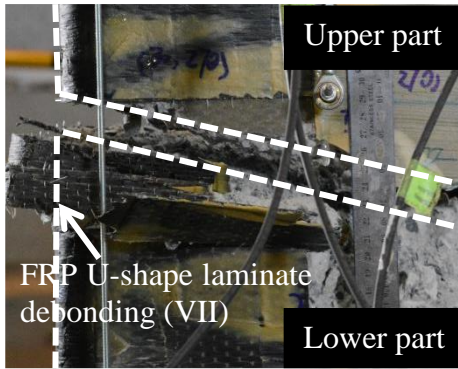
e) FRP U-shape laminate debonding of SW150-3.5α.

f) Rebar fracturing

g) FRP U-shape laminate rupture with side concrete crushing
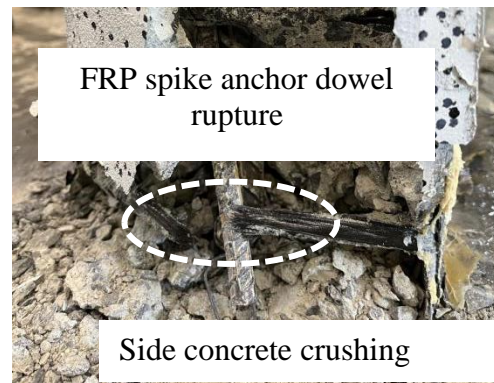
h) FRP spike anchor dowel rupture with side concrete crushing
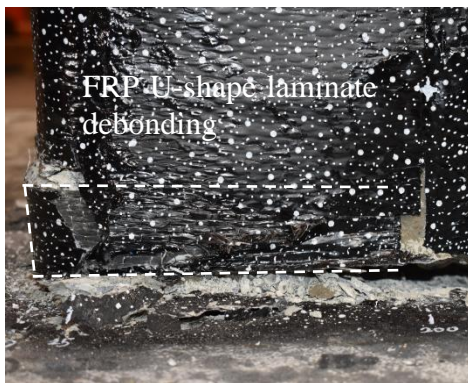
(i) FRP U-shape laminate debonding of SW150-10γ

(j) FRP spike anchor fan bulging

Figure 18 Test observations

The backbone curves of all the tested walls are compared in Figure 19. For the walls subjected to 10% axial load ratio, the improvement of the peak load was minimal, but the post-peak capacity was improvement considerably. For walls subjected to 3.5% axial load ratio, the improvement of the load behaviour was insignificant. The improvement in ductility is remarkable, with the walls reaching well over 2.5% drift without collapsing (the negative side

of the wall SW150-3.5α is a result of test setup issues). Further details are included in the attachments.
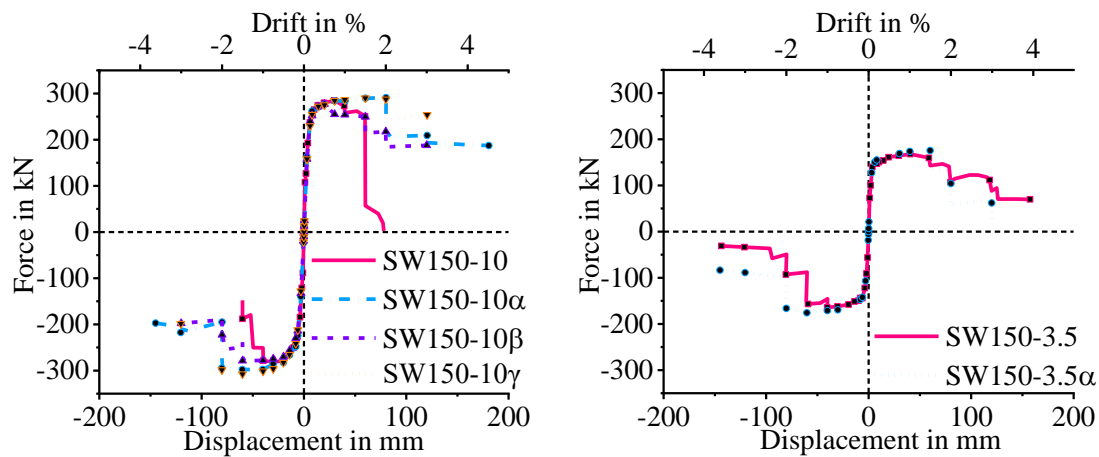
Figure 19 Backbone curves

Conclusions and key findings

We completed an exhaustive experimental and analytical study of the compression behaviour of concrete prisms confined with FRP materials and developed a design model to calculate the stress-strain response. The deformation capacity of the prisms can be significantly improved, but the anchors need to be placed close together. The model can predict the behaviour for the range of parameters investigated.

We then used the design model to strengthened thin and singly reinforced walls to prevent axial, brittle failure. All various FRP configurations significantly improved the deformation capacity and the ductility of the walls, shifting the failure from brittle, axial failure to flexurally dominated failure. While having a secondary confinement area does not significantly compromise the behaviour of the walls, they are recommended to provide further redundancy in case of premature failure of the primary confinement (e.g. installation error).

Future work

This project is still on-going, with the PhD candidate finishing the thesis and preparing the papers for publication (details below). This work does not require further funding. The PI is also scheduled to bring up these outputs to the American Concrete Institute, whose design guidelines are used in New Zealand in lieu of local design documents, to include the results in their ACI 440.2R document.

Outputs and dissemination

The list of outputs and dissemination is below, with all the documents being attached

Title	Venue	Progress/status
Axial Behavior of Concrete Prisms Confined by FRP Laminate and Spike Anchors	Journal of Composites for Construction by the American Society of Civil Engineer (ASCE-JCC)	Published
Axial Compression Testing of Concrete Prisms Confined by FRP Spike Anchors 1 and estimation of failure modes	ASCE-JCC	In pre-print
Stress-strain model of concrete confined by FRP laminate and spike anchors	ASCE-JCC	Completed and reviewing with co-authors
Testing of the pre-1970s singly reinforced concrete walls confined with FRP laminate and spike anchors to avoid axial failure	Engineering Structures	75%
Testing and design recommendations of confinement to wall ends with FRP laminate and spike anchors	Structural Engineering SOCiety (SESOC) conference, Hamilton 2021	Presented in 2021
Testing on concrete prisms confined by FRP laminate and spike anchors	The 15th International Conference on Fibre-Reinforced Polymers for Reinforced Concrete Structures (FRPRCS-15) & The 8th Asia-Pacific Conference on FRP in Structures (APFIS-2022) 10-14 December 2022, Shenzhen, China	Ready for submission to the conference committee
Seismic strengthening of RC walls using FRP to prevent axial failure	NZSEE conference 2023	Abstract submitted
TBD	SESOC Conference 2023	Call not open yet

Acknowledgements

Tables

Table 1 Test matrix for configuration A

Group ID	S (mm)	A_d (mm^2)	L_f (mm)	W_f (mm)	Repetitions
S					3
S90-28	90	28	122	90	4
S120-28	120	28	122	120	3
S180-28	180	28	122	180	3
S90-14	90	14	122	90	4
S120-14	120	14	122	120	4
S180-14	180	14	122	180	4
S120-56	120	56	122	120	1
S180-56	180	56	122	180	1
R					3
R90-28	90	28	172	90	4
R120-28	120	28	172	120	3
R180-28	180	28	172	180	3
R90-14	90	14	172	90	3
R120-14	120	14	172	120	3
R180-14	180	14	172	180	4
R120-56	120	56	172	120	1
R180-56	180	56	172	180	1

Table 2 Test matrix for configuration B

Group ID	S_d (mm)	A_d (mm^2)	L_f (mm)	W_f (mm)	Repetition
DS					1
S90-28	90	28	122	90	2
S120-28	120	28	122	120	2

S180-28	180	28	122	180	2
DR					2
DR90-28	90	28	172	90	2
DR120-28	120	28	172	120	2
DR180-28	180	28	172	180	2

Table 3 Concrete properties for configuration A

Age (days)	E_c (GPa)	f_c (MPa)	ε_c ($10^{-3}\varepsilon$)	f_t (MPa)	f_{ft} (MPa)	ρ_c (kg/m^3)
132	21.1	27.9	2.4	2.3	3.4	2285
260	21.6	28.2	2.0	3.1	3.1	2305
300	24.5	31.3	2.3	2.9		2317
312		31.5				2305
Ave	22.4	29.7	2.2	2.8	3.3	2302
SD	1.5	1.7	0.2	0.3	0.2	13.0
CoV (%)	6.8	5.6	7.3	12.5	4.6	0.6

Table 4 Concrete properties for configuration B

Properties	E_c (GPa)	f_c (MPa)	ε_c (10^{-3})	f_t (MPa)	f_{ft} (MPa)	ρ_c (kg/m^3)
AVE	26.3	36.7	2.3	3.5	4.5	2350
SD	1.7	0.9	0.1	0.4	0.3	13.2
CoV (%)	6.3	2.6	4.2	11.5	7.7	0.6

Table 5 FRP material properties

FRP product and statistics	Laminate			Anchor		
	AVE	SD	CoV (%)	AVE	SD	CoV (%)
Width of cured coupons (mm)	25.7	1.0	4.1	26.5	0.4	1.7
Thickness of dry products (mm)[a]		0.331				
Thickness of cured coupons (mm)	1.1	0.2	17.3	1.7	0.1	3.9
Area of dry products (mm^2)	8.5	0.3	3.8	14.7	1.8	12.2
Area of cured coupons (mm^2)	27.5	4.6	16.8	46.1	2.6	5.5
Elastic modulus of dry products (GPa)	234.4	19.8	8.4	236.4	3.2	1.3
Elastic modulus of cured coupons (GPa)	73.9	13.5	18.3	74.7	2.4	3.3
Ultimate strain of cured coupons (10^{-3})	11.0	1.4	12.7	11.8	0.3	2.9

[a] Provided by manufacturer

<div align="center">Table 6 Epoxy resin properties</div>

Properties	Temperature (Celsius)	Relative humidity (%)	Tensile strength (MPa)	Strain at rupture (10^{-3})
AVE	17.4	67.8	37.3	28.2
SD	0.6	9.5	1.9	5.3
CoV (%)	3.7	14.0	5.0	18.8

<div align="center">Table 7 Failure mode of confined prisms for confinement A</div>

Prism ID	FM	Prism ID	FM	Prism ID	FM	Prism ID	FM
S90-14-1	Fibre rupture	S90-28-1	Fibre rupture	R90-14-1	Fibre rupture	R90-28-1	Fibre rupture
S90-14-2	Fibre rupture	S90-28-2	Fibre rupture			R90-28-2	Fibre rupture
S90-14-3	Fibre rupture	S90-28-3	Fibre rupture	R90-14-2	Fibre rupture	R90-28-3	Fibre rupture
S90-14-4	Fibre rupture	S90-28-4	Debonding	R90-14-3	Fibre rupture	R90-28-4	Fibre rupture
S120-14-1	Fibre rupture	S120-28-1	Fibre rupture	R120-14-1	Fibre rupture	R120-28-1	Fibre rupture
S120-14-2	Fibre rupture	S120-28-2	Fibre rupture			R120-28-2	Fibre rupture
S120-14-3	Fibre rupture	S120-28-3	Fibre rupture	R120-14-2	Fibre rupture	R120-28-3	Fibre rupture
S120-14-4	Fibre rupture	S120-56-1	Concrete-controlled	R120-14-3	Fibre rupture	R120-56-1	Concrete-controlled
S180-14-1	Fibre rupture	S180-28-1	Fibre rupture	R180-14-1	Fibre rupture	R180-28-1	Fibre rupture
S180-14-2	Fibre rupture	S180-28-2	Fibre rupture	R180-14-2	Fibre rupture	R180-28-2	Fibre rupture
S180-14-3	Fibre rupture	S180-28-3	Fibre rupture	R180-14-3	Fibre rupture	R180-28-3	Fibre rupture
S180-14-4	Fibre rupture	S180-56-1	Concrete-controlled	R180-14-4	Fibre rupture	R180-56-1	Concrete-controlled

<div align="center">Table 8 Failure mode of confined prisms for confinement B</div>

Prism ID	Failure mode	Prism ID	Failure mode
DS90-28-1	Fibre rupture	DR90-28-1	Fibre rupture
DS90-28-2	Fibre rupture	DR90-28-2	Fibre rupture
DS90-28-3	Debonding	DR90-28-3	Fibre rupture

DS120-28-1	Fibre rupture	DR120-28-1	Concrete-controlled failure
DS120-28-2	Fibre rupture	DR120-28-2	Concrete-controlled failure
DS120-28-3	Fibre rupture	DR120-28-3	Concrete-controlled failure
DS180-28-1	Concrete-controlled failure	DR180-28-1	Concrete-controlled failure
DS180-28-2	Concrete-controlled failure	DR180-28-2	Concrete-controlled failure
DS180-28-3	Concrete-controlled failure	DR180-28-3	Concrete-controlled failure

Table 9 Mechanical properties of concrete for configuration A

Prism ID	$f_{co}(f_{cp})$ (MPa)	$\varepsilon_{co}(\varepsilon_{cp})$ $(10^{-3}\varepsilon)$	$f_{cu}(f_{ccu})$ (MPa)	$\varepsilon_{cu}(\varepsilon_{ccu})$ $(10^{-3}\varepsilon)$	$\dfrac{f_{cp,ave}}{f_{co,ave}}$	$\dfrac{\varepsilon_{cp,ave}}{\varepsilon_{co,ave}}$	$\dfrac{\varepsilon_{ccu,ave}}{\varepsilon_{cu,ave}}$
S-1	29.8	2.3	24.7	3.4			
S-2	29.0	2.5	25.8	3.5			
S-3	32.0	2.8	26.7	4.2			
S90-14-1	39.4	5.0	38.6	7.2			
S90-14-2	38.7	8.4	34.7	10.3	1.28	2.44	2.30
S90-14-3	39.1	5.5	38.4	6.2			
S90-14-4	38.0	5.7	37.4	10.2			
S120-14-1	34.9	5.6	32.0	7.8			
S120-14-2	36.6	5.6	34.6	6.8	1.22	2.23	2.49
S120-14-3	35.2	4.9	32.2	9.6			
S120-14-4	40.7	6.5	32.8	12.5			
S180-14-1	34.6	4.3	34.1	6.3			
S180-14-2	33.6	4.3	26.7	9.5	1.17	2.00	2.33
S180-14-3	37.9	6.0	35.6	7.9			
S180-14-4	35.2	5.6	28.1	10.7			
S90-28-1	41.1	9.3	41.1	9.3			
S90-28-2	39.4	9.8	39.4	9.8	1.31	3.96	2.98
S90-28-3	39.6	10.8	39.6	10.8			
S90-28-4	38.8	10.1	36.6	14.0			
S120-28-1	39.0	5.3	37.3	7.3	1.27	2.50	2.61

S120-28-2	37.3	7.0	33.6	12.6			
S120-28-3	39.2	6.6	38.7	8.9			
S120-56-1	42.7	5.8	28.2	19.8	1.41	2.28	5.38
S180-28-1	36.1	3.8	32.2	6.2			
S180-28-2	34.6	3.6	29.9	6.6	1.18	1.82	2.30
S180-28-3	36.6	6.4	31.7	12.6			
S180-56-1	41.9	4.3	29.1	7.4	1.38	1.69	2.02
R-1	32.0	2.7	28.2	4.9			
R-2	36.6	2.8	29.8	4.4			
R-3	32.1	2.4	25.1	3.6			
R90-14-1	44.3	4.4	36.8	9.1			
R90-14-2	40.5	3.7	31.5	9.6	1.44	1.52	2.35
R90-14-3	45.5	3.9	31.0	11.6			
R120-14-1	41.5	5.2	35.8	9.4			
R120-14-2	39.7	7.1	39.1	8.6	1.35	2.14	2.09
R120-14-3	41.4	4.7	34.5	9.0			
R180-14-1	41.1	4.6	31.7	9.4			
R180-14-2	34.8	4.0	29.9	7.8	1.27	1.57	2.02
R180-14-3	38.0	3.6	31.9	6.5			
R180-14-4	39.8	4.4	31.7	11.1			
R90-28-1	46.1	4.4	34.3	8.2			
R90-28-2	47.4	5.7	44.7	8.6	1.50	2.24	2.42
R90-28-3	44.1	7.0	41.4	10.4			
R90-28-4	43.6	6.7	31.4	14.4			
R120-28-1	38.7	7.9	34.3	14.7			
R120-28-2	38.7	6.6	35.1	9.9	1.27	2.44	3.19
R120-28-3	38.3	4.8	27.5	16.7			
R120-56-1	54.2	7.0	43.8	17.3	1.61	2.65	4.02
R180-28-1	35.2	3.7	29.2	7.6			
R180-28-2	40.0	4.6	36.0	9.7	1.27	1.69	2.01
R180-28-3	39.9	5.2	34.7	8.8			
R180-56-1	45.4	3.8	32.1	12.8	1.35	1.43	2.97

Table 10 Mechanical properties of test prisms

Prism ID	f_{co} (f_{cp}) (MPa)	ε_{co} (ε_{cp}) (10^{-3})	f_{cu} (f_{ccu}) (MPa)	ε_{cu} (ε_{ccu}) (10^{-3})	$\dfrac{f_{cp,ave}}{f_{co,ave}}$	$\dfrac{\varepsilon_{cp,ave}}{\varepsilon_{co,ave}}$	$\dfrac{\varepsilon_{ccu,ave}}{\varepsilon_{cu,ave}}$
DS-1	33.6	2.2	26.4	3.1			
DS-2	33.5	2.3	27.1	3.1			
DS90-28-1	35.2	4.4	28.4	15.4			
DS90-28-2	35.3	3.8	29.4	14.2	1.04	1.88	5.29
DS90-28-3	33.9	4.3	27.7	19.5			
DS120-28-1	35.2	4.2	28.3	10.6			
DS120-28-2	33.5	3.6	27.6	10.8	1.03	1.75	3.95
DS120-28-3	35.5	3.8	26.0	15.3			
DS180-28-1	32.4	2.4	25.7	4.8			
DS180-28-2	31.5	2.5	25.5	4.9	0.95	1.13	1.62
DS180-28-3	32.0	2.6	27.9	5.2			
DR-1	31.9	2.2	26.6	3.4			
DR-2	35.3	2.3	30.8	3.1			
DR-3	34.3	2.1	28.0	2.7			
DR90-28-1	34.4	5.3	27.5	14.6			
DR90-28-2	36.8	5.5	29.9	12.8	1.06	2.15	4.23
DR90-28-3	36.3	3.4	29.3	11.6			
DR120-28-1	35.8	3.9	26.8	7.8			
DR120-28-2	35.3	3.8	31.0	7.7	1.03	1.73	2.47
DR120-28-3	33.7	3.6	29.4	7.3			
DR180-28-1	36.6	2.9	30.0	5.8			
DR180-28-2	34.2	3.2	25.9	6.4	1.02	1.26	1.80
DR180-28-3	32.8	2.2	26.6	4.5			

Table 11 Wall test matrix

Wall ID	Axial load ratio (%)	Confinement configuration	
		Negative end (-)	Positive end (+)
SW150-10[a]	10		
SW150-10α	10	S90-28 and DS90-28	DS90-28 and S90-28
SW150-10β	10	Dual DS90-28	Dual DS90-28

SW150-10γ	10	R180-56	R90-28
SW150-3.5[a]	3.5		
SW150-3.5α	3.5	S90-28	S90-28

[a]Reference wall tested previously(Zhang et al. 2018b; Zhang 2019b).

Table 12 Concrete properties

Wall ID	ρ_c (kg/m^3)	E_c (GPa)	$f_c^{'}$ (MPa)	$\varepsilon_c^{'}$ (10^{-3})	f_t (MPa)
SW150-10[a]	2381	26.2	35.3	2.2	3.1
SW150-10α	2333.1	27.5	36.2	2.0	3.2
SW150-10β	2344.2	25.4	37.8	2.4	2.9
SW150-10γ	2332.0	29.7	42.4	2.2	3.9
SW150-3.5[a]	2370	29.5	36.3	2.1	3.0
SW150-3.5α	2236.2	25.5	36.5	2.4	2.5

[a]Tested previously(Zhang et al. 2018b; Zhang 2019b).

Table 13 Rebar properties

Rebar	Properties	f_y (MPa)	ε_y (10^{-3})	ε_h (10^{-3})	f_u (MPa)	ε_u (10^{-3})
D10	Reference walls[a]	286.6	1.4		399.5	180.0
	Strengthened walls	338.2	1.7		450.7	189.4
D16	Reference walls[a]	294.7	1.5	20.3	451.2	195.4
	Strengthened walls	301.6	1.5	22.2	415.9	225.3

[a]Tested previously(Zhang et al. 2018b; Zhang 2019b).

References

ACI (American Concrete Institute). 2007. "*Acceptance criteria for specialunbonded post-tensioned precast structural walls based on validationtesting and commentary*." ACI ITG-5.1-07. Detroit.

ACI (American Concrete Institute). 2017. "*Guide for the Design and Construction of Externally Bonded FRP Systems for Strengthening Concrete Structures*." ACI 440.2R. Farming Hills, Michigan, U.S.A.

Altin, S., Anil, Ö., Kopraman, Y., and Kara, M. E. 2013. "Hysteretic behavior of RC shear walls strengthened with CFRP strips." *Composites Part B: Engineering*, 44(1), 321-329.

Dan, D. 2012. "Experimental tests on seismically damaged composite steel concrete walls retrofitted with CFRP composites." *Engineering structures*, 45, 338-348.

del Rey Castillo, E., Griffith, M., and Ingham, J. 2018. "Seismic behavior of RC columns flexurally strengthened with FRP sheets and FRP anchors." *Composite Structures*, 203, 382-395.

El-Sokkary, H., Galal, K., Ghorbanirenani, I., Léger, P., and Tremblay, R. 2013. "Shake table tests on FRP-rehabilitated RC shear walls." *Journal of Composites for Construction*, 17(1), 79-90.

Fardis, M. N., and Khalili, H. H. 1982. "FRP-encased concrete as a structural material." *Magazine of concrete research*, 34(121), 191-202.

Kalfat, R., and Al-Mahaidi, R. 2016. "Improvement of FRP-to-concrete bond performance using bidirectional fiber patch anchors combined with FRP spike anchors." *Composite Structures*, 155, 89-98.

Kam, W. Y., and Pampanin, S. 2011. "The seismic performance of RC buildings in the 22 February 2011 Christchurch earthquake." *Structural Concrete*, 12(4), 223-233.

Khalil, A., and Ghobarah, A. 2005. "Behaviour of rehabilitated structural walls." *Journal of earthquake engineering*, 9(3), 371-391.

Kobayashi, K. 2005. "Innovative application of FRPs for seismic strengthening of RC shear wall." *Proceeding, Fiber-Reinforced Polymer (FRP) Reinforcement for Concrete Structures*, 1269-1288.

Lam, L., and Teng, J. 2003. "Design-oriented stress-strain model for FRP-confined concrete in rectangular columns." *Journal of reinforced plastics and composites*, 22(13), 1149-1186.

MATLAB 2015. *MATLAB and statistics toolbox release 2015*, Natick, Massachusetts, United States: The MathWorks Inc.

Matsui, T., Saito, T., and Reyna, R. 2014. "Basic study on reinforced concrete shear walls without boundary columns retrofitted by carbon fiber sheets." *Journal of Disaster Research*, 9(6), 1008-1014.

Matsui, T., Saito, T., and Reyna, R. 2017 "Structural performance of rectangular reinforced concrete walls retrofitted by carbon fiber sheets." *Proc., 16th World Conference on Earthquake Engineering, Santiago, January*, 9-13.

Moran, D. A., Pantelides, C. P., and Reaveley, L. D. 2019. "Mohr-coulomb model for rectangular and square FRP-confined concrete." *Composite Structures*, 209, 889-904.

Paulay, T., and Priestley, M. N. 1992. *Seismic design of reinforced concrete and masonry buildings*.

Qazi, S. 2013. "Mechanical behavior of RC walls under seismic activity strenghtened with CFRP." INSA de Lyon.

Qazi, S., Michel, L., and Ferrier, E. 2015. "Impact of CFRP partial bonding on the behaviour of short reinforced concrete wall under monotonic lateral loading." *Composite Structures*, 128, 251-259.

Shegay, A., Dashti, F., Hogan, L., Lu, Y., Niroomandi, A., Seifi, P., Zhang, T., Dhakal, R., Elwood, K., and Henry, R. 2020. "Research programme on seismic performance of reinforced concrete walls." *Bulletin of the New Zealand Society for Earthquake Engineering*, 53(2), 54-69.

Sritharan, S., Beyer, K., Henry, R. S., Chai, Y., Kowalsky, M., and Bull, D. 2014. "Understanding poor seismic performance of concrete walls and design implications." *Earthquake Spectra*, 30(1), 307-334.

Stubbing, R. 2013. "Characterisation of polymeric foam cores using digital image correlation." Ph.D. thesis, University of Auckland.

Stubbing, R. M. 2016. *DTA Report 408/NR 1690-Digital Image Correlation Capability*, Defence Technology Agency (DTA), New Zealand Defence Force.

Zhang, T. 2019a. "Seismic Assessment of Reinforced Concrete Walls in Pre-1970s Multi-Storey Buildings." Ph.D. thesis, University of Auckland, Auckland, New Zealand.

Zhang, T. 2019b. "Seismic Assessment of Reinforced Concrete Walls in Pre-1970s Multi-Storey Buildings." Ph.D. thesis, University of Auckland, Auckland, New Zealand.

Zhang, T., Elwood, K., and Henry, R. 2018a "Testing of singly reinforced concrete walls used in existing buildings." *Proc., 2018 NZSEE Annual Conference*, 1-8.

Zhang, T., Elwood, K., and Henry, R. 2018b "Testing of singly reinforced concrete walls used in existing buildings." *Proc., 2018 NZSEE Annual Conference*.